UCSF
UC San Francisco Electronic Theses and Dissertations

Title
Activation and assembly of RNA decay factors by Pat1

Permalink
https://escholarship.org/uc/item/644045jd

Author
Lobel, Joseph Heimlich

Publication Date
2020

Peer reviewed|Thesis/dissertation

eScholarship.org Powered by the California Digital Library
University of California

Activation and assembly of RNA decay factors by Pat1

by
Joseph Heimlich Lobel

DISSERTATION
Submitted in partial satisfaction of the requirements for degree of
DOCTOR OF PHILOSOPHY

in

Chemistry and Chemical Biology

in the

GRADUATE DIVISION
of the
UNIVERSITY OF CALIFORNIA, SAN FRANCISCO

Approved:

DocuSigned by:
John D Gross
C876331A93DC4B1...

John D Gross
Chair

DocuSigned by:
Geeta Narlikar
[illegible]43B...

Geeta Narlikar

DocuSigned by:
Hiten Madhani
76DDD3CF67EA4D0...

Hiten Madhani

Committee Members

Copyright 2020

by

Joseph Heimlich Lobel

Acknowledgements

There are numerous people who have been vital to completing the research described in this dissertation, who have all helped in a significant manner at both the personal and professional level. First, my endless gratitude goes to my thesis advisor Dr. John Gross, who allowed me to develop my own project and gave me a degree of independence that, though challenging at times, has made me more fearless in tackling important biological problems. Furthermore, I'm grateful for the feedback on presentations and writing that he has provided, which has been invaluable for my long-term scientific development. I would also like to thank members of the Gross lab for scientific discussion and experimental guidance, especially those involved on the decapping project. More broadly, UCSF has an incredible community of people and scientists who I've had the pleasure of befriending during graduate school. I would particularly like to thank Drs. Daniel Elnatan, Sam Ivry, Nathan Gamarra, Alex Martinko, Rose Citron, Andrew Lyon, Miguel Betegon, Elaine Kirschke, and Adam Larson, who have been great to know both inside and outside of the lab. I am very lucky to have a wonderful group of friends and mentors during my doctoral studies.

On a personal level, my family has been a source of relief and comfort during graduate school. My parents Diane Heimlich and Peter Lobel, brother Sam Lobel, Aunt Judith Heimlich, and Uncle Jon Weintraub have been enormous parts of everything, and would require too many pages to adequately express my gratitude. The same can be said about my partner, Sara Calhoun, who has endured all my ups and downs during my graduate studies. It is a joy to experience her humor, intelligence, and compassion and I am excited to continue growing with her during the next phase of our lives.

Abstract

Activation and assembly of RNA decay factors by Pat1

Joseph Heimlich Lobel

Bulk RNA degradation irreversibly removes an mRNA from the translating pool to regulate gene expression. A dense network of proteins assembles on a transcript to ensure timely and specific destruction of the RNA. The first steps of bulk mRNA degradation begin with the trimming of the 3' poly(A) tail followed by removal of the 5' methyl-7 guanine (m^7G) cap structure, leading to rapid exonucleolysis of the message. A key question has been understanding how protein factors at the 3' end trigger decapping at the 5' end. Pat1 is a central scaffolding protein that interacts with both the 5' decapping machinery and the 3' Lsm1-7 complex to control distinct steps during RNA turnover. Due to the multifunctional nature of Pat1, however, we lack a mechanistic understanding of how it regulates RNA turnover. In this work, I have used a reconstituted system to understand how Pat1 interacts with and activates distinct factors during 5'-3' degradation. First, I show how Pat1 interacts with and enhances the RNA binding of Lsm1-7. This increased affinity is selective for adenine-rich oligoRNAs, which broadens the target specificity of the Lsm1-7 complex. Second, I show how Pat1 interacts with short linear motifs in the disordered C-terminal tail of Dcp2 to activate decapping by recruiting the enzyme complex to substrate and alleviating autoinhibition to promote catalysis. Both activation of Lsm1-7 and decapping require a bipartite interaction between two domains of Pat1 and involve distinct surfaces and motifs. Last, I uncover how different decay factors tune both the size and assembly of Pat1, which may be leveraged to organize an active decapping mRNP. This biochemically reconstituted system provides a framework for how Pat1 can regulate multiple protein cofactors and steps during bulk RNA turnover.

Table of Contents

List of Figures

Chapter 1

Chapter 2

Chapter 3

List of Tables

Chapter 1

Chapter 2

Chapter 3

Introduction

All RNAs undergo extensive processing and compositional changes during their lifetime, from transcription and splicing, to translation, and ultimately to decay (Moore 2005). The fate of the mRNA strongly depends on the RNA binding proteins (RBPs) that decorate the transcript, which bind both sequence and structural moieties in the body of the message, as well as the 5' methyl-7-gaunine cap (m7G) and the 3' poly-adenine tail terminal features. The RBP composition of a transcript changes during its lifecycle to orchestrate distinct processes, and different RBPs communicate with each other, as well as features at the 5' and 3' of the message, to influence RNA processing. Thus, understanding how RBPs interact with each other and with the RNA is critical to understanding post-transcriptional gene regulation.

A major form of post transcriptional control of gene expression involves degradation of the mRNA. By removing the transcript from the translating pool, RNA degradation ensures timely and specific quantity of gene expression and is important for many physiological processes, such as development, cell growth, and antiviral responses (Parker 2012). Cleavage of the 5' m^7G cap (decapping) removes the transcript from the translating pool by leading to rapid 5'-'3 degradation by conserved exonucleases (Dunckley and Parker 1999; Van Dijk et al. 2002; Wang et al. 2002). The importance of decapping is underscored by multiple mRNA decay pathways converging on this step, including microRNA (miRNA) mediated decay, bulk mRNA decay, and different quality control mechanisms (Guo et al. 2010; Kurosaki et al. 2019; Parker 2012). Decapping is largely irreversible, and thus highly regulated by a dense network of protein factors that coordinate multiple activities across the transcript to control degradation.

Bulk 5'-3' mRNA decay begins with the trimming of the poly(A) by cytoplasmic deadenylases such as the CCR4/NOT or Pan2/3 deadenylase complex (Muhlrad et al. 1994; Mugridge et al. 2018). Deadenylation leads to loss of translational initiation machinery and permits the assembly of a decapping messenger RNA ribonucleic acid protein (mRNP) complex. The conserved heteroheptameric Lsm1-7 complex binds to the 3' deadenylated tail with the scaffolding protein Pat1, which subsequently recruits the 5' decapping complex to the transcript, leading to decapping (Tharun et al. 2000; Bouveret 2000; Tharun and Parker 2001; Nissan et al. 2010). After decapping, the 5'-3' exonuclease, Xrn1, cotranslationally degrades the mRNA (Tesina et al. 2019; Chang et al. 2019; Jinek et al. 2011; Pelechano et al. 2015). Proper 5'-3' decay clearly involves association of numerous factors, and a major question has been reconciling how initial decay events at the 3' end (deadenylation and Lsm1-7 binding) promotes activities at the 5' end (decapping and degradation). A detailed description of each of these processes and involved complexes is described below. Understanding how 5' and 3' events are linked will improve our mechanistic understanding about how unique cofactors promote different steps of decay.

The heteroheptameric Lsm1-7 complex binds to the 3' oligo(A) tail after deadenylation (Chowdhury et al. 2007; Tharun and Parker 2001). Much work has been done on the *Saccharomyces Cerevisiae* Lsm1-7 complex, which has the inherent preference to bind oligo(A) tails over longer poly(A) tails. Lsm1-7 consists of 7 small Like-Sm proteins that all have a similar β-sheet fold that assemble into a donut shape (Sharif and Conti 2013; Chowdhury et al. 2007; Zhou et al. 2014). Lsm1 has a C-terminal α-helix that spans the ring and may regulate RNA binding (Sharif and Conti 2013; Tharun et al. 2005; Chowdhury et al. 2013). Deletion of Lsm1 stabilizes inefficiently translated mRNAs, suggesting it somehow senses, likely indirectly, the translation

status of the mRNA (He et al. 2018; Rissland and Norbury 2009; Wang et al. 2017). Furthermore, deletion of Lsm1 results in mRNAs with trimmed 3' untranslated regions (UTRs), indicating it blocks 3'-5' decay pathways and may help kinetically drive 5' decapping (He and Parker 2001). In metazoans and some fungi, like *Schizosaccroymces pombe*, an additional 1-3 uracil nucleotides can be added to deadenylated tails, which are also substrates for Lsm1-7 and help mark a transcript for destruction (Rissland and Norbury 2009; Chang et al. 2014). The scaffolding protein Pat1 functionally regulates Lsm1-7 RNA binding and forms a tight interaction with the heteroheptameric ring (Chowdhury et al. 2013; Lobel et al. 2019; Sharif and Conti 2013). The Pat1/Lsm1-7 interaction is required for proper function *in vivo*, but how this heterooctameric complex functions is poorly understood.

Decapping by Dcp2 the 5' end sentences an mRNA to rapid degradation and thus is a major point of regulation. The Dcp1/Dcp2 complex consists of two parts essential for activity: Dcp1 is an EVH1 domain protein the interacts with cofactors via proline recognition and enhances activity of the catalytic subunit, Dcp2 (Borja et al. 2011; Mugridge et al.). Dcp2 is bilobed NUDIX hydrolase the contains a conserved dynamic catalytic core that recognizes and cleaves the cap, and in fungi, a long disordered C-terminal extension that contains autoinhibitory elements and specific protein-protein interaction motifs known as helical leucine motifs (HLMs) (Floor et al. 2010; He and Jacobson 2015; Fromm et al. 2012). Different activators can enhance decapping by multiple mechanisms, either by binding the catalytic core to promote an active conformation of the enzyme or by binding HLMs to alleviate autoinhibition (Paquette et al. 2018; Wurm et al. 2017). Because decapping is a final commitment to degradation, it is paramount to understand how RNA decay factors regulate the activity of Dcp1/Dcp2.

It is thought that an RNA decay factor must bridge 3' oligo(A) binding and 5' decapping to relay deadenylation to decapping. A prime candidate to do this is the scaffolding protein Pat1, which functionally interacts with numerous RNA decay factors during 5'-3' mRNA decay (Nissan et al. 2010; Sharif et al. 2013; Sharif and Conti 2013; Charenton et al. 2017). Studying Pat1's function, however, has remained challenging because it is involved in numerous post-transcriptional processes, from splicing to translation repression to RNA turnover (Coller and Parker 2005; Haas et al. 2010; Braun et al. 2010; Bonnerot et al. 2000). Many lines of evidence suggest that Pat1 may be the bridge between the 5' and 3' ends of the transcript during bulk mRNA degradation. First, deletion of Pat1 and Lsm1-7 stabilize nearly an identical set of poorly translated RNAs, suggesting Pat1 and Lsm1-7 act as a complex (He et al. 2018). Second, deletion of Pat1 results in the accumulation of capped, deadenylated transcripts, suggesting Pat1 functions after Lsm1-7 binding but prior to decapping (Wang et al. 2017). Third, biochemical and biophysical evidence suggest direct interactions between Pat1 and both the Lsm1-7 ring and the Dcp1/Dcp2 complex (Lobel et al. 2019; Charenton et al. 2017; Sharif and Conti 2013). Finally, Pat1 is a core component of Processing-Bodies (P-Bodies), which are a class of phase separated membrane-less organelles that contain both 5' and 3' mRNA decay factors, including Lsm1-7 and Dcp1/Dcp2 (Xing et al. 2018; Teixeira and Parker 2007). Because Pat1 makes interactions with many different decay factors, it is a prime candidate to link both 5' and 3' activities during bulk mRNA degradation. Understanding how Pat1 functions in RNA decay will illuminate how multiple protein cofactors are coordinate to promote timely and specific decapping of target transcripts.

From fungi to metazoans, Pat1 has three domains that make contacts with different cofactors. The disordered N-terminal domain contains a conserved FDF motif that interacts with the DEAD-box

helicase Dhh1 (DDX6 in humans), though deletion of this region has little effect on Pat1's function (Pilkington and Parker 2008; Sharif et al. 2013). The disordered middle domain is the most conserved part of Pat1 and is required for decapping, but the molecular functions have remained elusive (Lobel et al. 2019; Pilkington and Parker 2008). Finally, the globular C-terminal domain makes contacts with the Lsm1-7 complex via the Lsm2/3 subunits and, in fungi, binds HLMs in Dcp2 (Wu et al. 2014; Charenton et al. 2017). The combination of the middle and C-terminal domains is the minimal construct to support normal growth in fungi (Lobel et al. 2019; Pilkington and Parker 2008). Furthermore, deletion of either the middle or C-terminal domains results in growth defects, hinting that these domains likely cooperate to promote normal mRNA turnover (Lobel et al. 2019). Thus, a mechanistic framework for decapping requires understanding how the unstructured middle domain of Pat1 cooperates with the globular C-terminal domain to regulate multiple decay steps.

In this dissertation, I describe my efforts to understand how Pat1 flips multiple molecular switches during decapping to regulate 5'-3' decay. To do this, I used a reconstituted system of recombinant Pat1 constructs and dissected how it interacted with the 3' Lsm1-7 complex and 5' Dcp1/Dcp2 holoenzyme. First, I show that Pat1 uses short linear motifs in the unstructured middle domain to activate enhance Lsm1-7 RNA binding and decapping by Dcp1/Dcp2. Second, I uncover how Pat1 broadens the RNA target repertoire of the Lsm1-7 complex. Finally, I find that different RNAs and cofactors tune the assembly of Pat1 from defined oligomers to micron-scale droplets. The combination of biochemical, biophysical, and genetic approaches used here elucidate the role of Pat1 in RNA turnover, with implications for how multiple protein interactions regulate distinct steps of 5'-3'mRNA decay.

References

Bonnerot C, Boeck R, Lapeyre B. 2000. The Two Proteins Pat1p (Mrt1p) and Spb8p Interact In Vivo, Are Required for mRNA Decay, and Are Functionally Linked to Pab1p. *Mol Cell Biol* **20**: 5939–5946.

Borja MS, Piotukh K, Freund C, Gross JD. 2011. Dcp1 links coactivators of mRNA decapping to Dcp2 by proline recognition. *RNA* **17**: 278–290.

Bouveret E. 2000. A Sm-like protein complex that participates in mRNA degradation. *EMBO J* **19**: 1661–1671.

Braun JE, Tritschler F, Haas G, Igreja C, Truffault V, Weichenrieder O, Izaurralde E. 2010. The C-terminal α-α superhelix of Pat is required for mRNA decapping in metazoa. *EMBO J* **29**: 2368–2380.

Chang C, Muthukumar S, Weber R, Levdansky Y, Chen Y, Bhandari D, Igreja C, Wohlbold L, Valkov E, Izaurralde E. 2019. A low-complexity region in human XRN1 directly recruits deadenylation and decapping factors in 5 – 3 messenger RNA decay. 1–14.

Chang H, Lim J, Ha M, Kim VN. 2014. TAIL-seq: Genome-wide Determination of Poly(A) Tail Length and 3' End Modifications. *Mol Cell* **53**: 1044–1052.

Charenton C, Gaudon-Plesse C, Fourati Z, Taverniti V, Back R, Kolesnikova O, Séraphin B, Graille M. 2017. A unique surface on Pat1 C-terminal domain directly interacts with Dcp2 decapping enzyme and Xrn1 5′–3′ mRNA exonuclease in yeast. *Proc Natl Acad Sci* **114**: E9493–E9501.

Chowdhury A, Kalurupalle S, Tharun S. 2013. Pat1 contributes to the RNA binding activity of the Lsm1-7 – Pat1 complex. *RNA* **20**: 1465–1475.

Chowdhury A, Mukhopadhyay J, Tharun S. 2007. The decapping activator Lsm1p-7p-Pat1p complex has the intrinsic ability to distinguish between oligoadenylated and polyadenylated

RNAs. *RNA* **13**: 998–1016.

Coller J, Parker R. 2005. General translational repression by activators of mRNA decapping. *Cell* **122**: 875–886.

Dunckley T, Parker R. 1999. The DCP2 protein is required for mRNA decapping in Saccharomyces cerevisiae and contains a functional MutT motif. *EMBO J* **18**: 5411–5422.

Floor SN, Jones BN, Hernandez GA, Gross JD. 2010. A split active site couples cap recognition by Dcp2 to activation. *Nat Struct Mol Biol* **17**: 1096–1101.

Fromm SA, Truffault V, Kamenz J, Braun JE, Hoffmann NA, Izaurralde E, Sprangers R. 2012. The structural basis of Edc3-and Scd6-mediated activation of the Dcp1:Dcp2 mRNA decapping complex. *EMBO J* **31**: 279–290.

Guo H, Ingolia NT, Weissman JS, Bartel DP. 2010. Mammalian microRNAs predominantly act to decrease target mRNA levels. *Nature* **466**: 835–840.

Haas G, Braun JE, Igreja C, Tritschler F, Nishihara T, Izaurralde E. 2010. HPat provides a link between deadenylation and decapping in metazoa. *J Cell Biol* **189**: 289–302.

He F, Celik A, Wu C, Jacobson A. 2018. General decapping activators target different subsets of inefficiently translated mRNAs. *Elife* **7**: 1–30.

He F, Jacobson A. 2015. Control of mRNA decapping by positive and negative regulatory elements in the Dcp2 C-terminal domain. *RNA* 1633–1647.

He W, Parker R. 2001. The yeast cytoplasmic lsm1/pat1p complex protects mRNA 3′ termini from partial degradation. *Genetics* **158**: 1445–1455.

Jinek M, Coyle SM, Doudna JA. 2011. Coupled 5’ Nucleotide Recognition and Processivity in Xrn1-Mediated mRNA Decay. *Mol Cell* **41**: 600–608.

Kurosaki T, Popp MW, Maquat LE. 2019. Quality and quantity control of gene expression by

nonsense- mediated mRNA decay. *Nat Rev Mol Cell Biol* **20**: 406–420.

Lobel JH, Tibble RW, Gross JD. 2019. Pat1 activates late steps in mRNA decay by multiple mechanisms. *Proc Natl Acad Sci* **116**: 23512–23517.

Moore MJ. 2005. From birth to death: The complex lives of eukaryotic mRNAs. *Science (80-)* **309**: 1514–1518.

Mugridge JS, Coller J, Gross JD. 2018. Structural and molecular mechanisms for the control of eukaryotic 5′–3′ mRNA decay. *Nat Struct Mol Biol* **25**.

Mugridge JS, Tibble RW, Ziemniak M, Jemielity J, Gross JD. Structure of the activated Edc1-Dcp1-Dcp2-Edc3 mRNA decapping complex with substrate analog poised for catalysis. *Nat Commun*.

Muhlrad D, Decker CJ, Parker R. 1994. Deadenylation of the unstable mRNA encoded by the yeast MFA2 gene leads to decappmg followed by 5'-> 3' digestion of the transcript. *Genes Dev* **8**: 855–866.

Nissan T, Rajyaguru P, She M, Song H, Parker R. 2010. Decapping Activators in Saccharomyces cerevisiae Act by Multiple Mechanisms. *Mol Cell* **39**: 773–783.

Paquette DR, Tibble RW, Daifuku TS, Gross JD. 2018. Control of mRNA decapping by autoinhibition. 1–12.

Parker R. 2012. RNA degradation in Saccharomyces cerevisae. *Genetics* **191**: 671–702.

Pelechano V, Wei W, Steinmetz LM. 2015. Widespread co-translational RNA decay reveals ribosome dynamics. *Cell* **161**: 1400–1412.

Pilkington GR, Parker R. 2008. Pat1 Contains Distinct Functional Domains That Promote P-Body Assembly and Activation of Decapping. *Mol Cell Biol* **28**: 1298–1312.

Rissland OS, Norbury CJ. 2009. Decapping is preceded by 3' uridylation in a novel pathway of

bulk mRNA turnover. *Nat Struct Mol Biol* **16**.

Sharif H, Conti E. 2013. Architecture of the Lsm1-7-Pat1 Complex: A Conserved Assembly in Eukaryotic mRNA Turnover. *Cell Rep* **5**: 283–291.

Sharif H, Ozgur S, Sharma K, Basquin C, Urlaub H, Conti E. 2013. Structural analysis of the yeast Dhh1-Pat1 complex reveals how Dhh1 engages Pat1, Edc3 and RNA in mutually exclusive interactions. *Nucleic Acids Res* **41**: 8377–8390.

Teixeira D, Parker R. 2007. Analysis of P-Body Assembly in Saccharomyces Cerevisiae. *Mol Biol Cell* **18**: 2274–2287.

Tesina P, Lessen LN, Buschauer R, Cheng J, Wu CC, Berninghausen O, Allen R, Becker T, Beckmann R, Green R. 2019. Molecular mechanism of translational stalling by inhibitory codon combinations and poly (A) tracts. *bioRxiv* 1–24.

Tharun S, He W, Mayes AE, Lennertz P, Beggs JD, Parker R. 2000. Yeast Sm-like proteins function in mRNA decapping and decay. *Nature* **404**: 515–518.

Tharun S, Muhlrad D, Chowdhury A, Parker R. 2005. Mutations in the Saccharomyces cerevisiae LSM1 gene that affect mRNA decapping and 3′ end protection. *Genetics* **170**: 33–46.

Tharun S, Parker R. 2001. Targeting an mRNA for decapping: Displacement of translation factors and association of the Lsm1p-7p complex on deadenylated yeast mRNAs. *Mol Cell* **8**: 1075–1083.

Van Dijk E, Cougot N, Meyer S, Babajko S, Wahle E, Séraphin B. 2002. Human Dcp2: A catalytically active mRNA decapping enzyme located in specific cytoplasmic structures. *EMBO J* **21**: 6915–6924.

Wang C-Y, Wang Y-T, Hsiao W-Y, Wang S-W. 2017. Involvement of fission yeast Pdc2 in

RNA degradation and P-body function. *RNA* **23**: 493–503.

Wang Z, Jiao X, Carr-Schmid A, Kiledjian M. 2002. The hDcp2 protein is a mammalian mRNA decapping enzyme. *Proc Natl Acad Sci* **99**: 12663–12668.

Wu D, Muhlrad D, Bowler MW, Jiang S, Liu Z, Parker R, Song H. 2014. Lsm2 and Lsm3 bridge the interaction of the Lsm1-7 complex with Pat1 for decapping activation. *Cell Res* **24**: 233–246.

Wurm JP, Holdermann I, Overbeck JH, Mayer PHO, Sprangers R. 2017. Changes in conformational equilibria regulate the activity of the Dcp2 decapping enzyme. *Proc Natl Acad Sci* **114**: 6034–6039.

Xing W, Muhlrad D, Parker R, Rosen MK. 2018. A quantitative inventory of yeast P body proteins reveals principles of compositional specificity. *bioRxiv*.

Zhou L, Zhou Y, Hang J, Wan R, Lu G, Yan C, Shi Y. 2014. Crystal structure and biochemical analysis of the heptameric Lsm1-7 complex. *Cell Res* **24**: 497–500.

Chapter 1

Pat1 activates late steps in mRNA decay by multiple mechanisms

Joseph H. Lobel[1,2], Ryan W. Tibble[1,2], John D. Gross[2,*]

[1]Chemistry and Chemical Biology Graduate Program, University of California, San Francisco, San Francisco, California

[2]Department of Pharmaceutical Chemistry, University of California, San Francisco, San Francisco, California

This chapter is adapted from:
Lobel, JH, Tibble, RW, Gross, JD. 2019. Pat1 activates late steps in mRNA decay by multiple mechanisms *Proc Natl Acad Sci* **116**: 23512 – 23517.

Abstract

Pat1 is a hub for mRNA metabolism, acting in pre-mRNA splicing, translation repression and mRNA decay. A critical step in all 5'-3' mRNA decay pathways is removal of the 5' cap structure, which precedes and permits digestion of the RNA body by conserved exonucleases. During bulk 5'-3' decay, the Pat1/Lsm1-7 complex engages mRNA at the 3' end and promotes hydrolysis of the cap structure by Dcp1/Dcp2 at the 5' end through an unknown mechanism. We reconstitute Pat1 with 5' and 3' decay factors and show how it activates multiple steps in late mRNA decay. First, we find that Pat1 stabilizes binding of the Lsm1-7 complex to RNA using two conserved short-linear interaction motifs. Secondly, Pat1 directly activates decapping by binding elements in the disordered C-terminal extension of Dcp2, alleviating autoinhibition and promoting substrate binding. Our results uncover the molecular mechanism of how separate domains of Pat1 coordinate the assembly and activation of a decapping mRNP that promotes 5'-3' mRNA degradation.

Introduction

Proper degradation of mRNA transcripts shapes the timing and quantity of gene expression to regulate a diverse array of cellular processes (Parker 2012; Moore 2005). Cleavage of the 5' m^7G cap (decapping) removes the mRNA from the translating pool and exposes a free monophosphate which leads to rapid degradation by the 5'-3' exonuclease Xrn1(Moore 2005; Stevens 1980). Decapping is a critical process for establishing 5'-3' mRNA degradation and is found in bulk mRNA decay, clearance of maternal transcripts, quality control pathways, and miRNA mediated decay (Guo et al. 2010; Jonas and Izaurralde 2015; Franks and Lykke-Andersen 2008; Kervestin and Jacobson 2012). The Dcp1/Dcp2 holoenzyme is a conserved NUDIX hydrolase that cleaves the 5' m^7G cap and is targeted to specific mRNAs by cofactors (Van Dijk et al. 2002; Parker 2012; Dunckley and Parker 1999; Badis et al. 2004; Dong et al. 2007; He et al. 2018; Wang et al. 2002).

These cofactors regulate the activity of Dcp1/Dcp2 by either binding the catalytic core of the enzyme or helical leucine motifs (HLMs) in the disordered C-terminus of Dcp2, which contains additional *cis*-regulatory elements that inhibit decapping (Mugridge et al.; Fromm et al. 2012; He and Jacobson 2015; Paquette et al. 2018). Thus, a dense network of protein interactions has evolved to coordinate decapping of specific mRNA targets (Jonas and Izaurralde 2013).

Bulk 5'-3' mRNA degradation begins with trimming of the 3' poly(A) tail, which may be followed by the addition of 1-3 uridines by terminal urdiyl transferases in higher order eukaryotes (Rissland and Norbury 2009; Lim et al. 2014). Deadenylation results in loss of translation initiation factors and permits the assembly of a decapping mRNP (Tharun and Parker 2001). Pat1 and Lsm1-7 work as a complex that assembles at the 3' end of an mRNA to subsequently promote decapping by Dcp1/Dcp2 (Tharun et al. 2000; Bouveret 2000; He and Parker 2001; Tharun et al. 2005; Tharun and Parker 2001; Bonnerot et al. 2000). Structural and biochemical studies have demonstrated that Pat1 and Lsm1-7 form a heterooctameric complex that engages transcripts containing oligoA tails that result from deadenylation (Sharif and Conti 2013; Wu et al. 2014; Chowdhury et al. 2007; Mitchell et al. 2012). Pat1 and Lsm1-7 are functionally linked, as they bind the 3' end of mRNA and deletion of either Pat1 or Lsm1 causes an increase in steady-state levels of numerous overlapping transcripts (He et al. 2018; Mitchell et al. 2012). In addition, deletion of Pat1 or Lsm1 results in an accumulation of deadenylated, capped mRNA intermediates, suggesting a block in decapping (Wang et al. 2017; Tharun and Parker 2001; Tharun et al. 2000). Finally, Pat1 forms a core component of P-bodies and can recruit interacting partners to these cytoplasmic foci, which may function in mRNA storage or decay (Youn et al. 2018; Hubstenberger et al. 2017; Teixeira and Parker 2007). A critical and unresolved question is how Pat1 coordinates assembly of Lsm1-7 complex on the mRNA 3' end with decapping at the 5' end.

Pat1 is conserved from yeast to humans and contains three domains that interact with distinct decay factors. The disordered N-terminal region of Pat1 contains a conserved motif that interacts with the DEAD-box ATPase Dhh1, but is generally dispensable for cell growth and normal mRNA turnover (Sharif et al. 2013; Pilkington and Parker 2008). The α-α superhelical C-terminal domain (PatC) interacts with Lsm1-7, which is required for bulk 5'-3' mRNA degradation *in vivo* (Wu et al. 2014; Chowdhury et al. 2013; Sharif and Conti 2013; Braun et al. 2010; Fourati et al. 2014). Removal of the unstructured middle domain severely attenuates decapping and 5'-3' degradation, though the mechanism remains poorly understood (Pilkington and Parker 2008; Haas et al. 2010). The conservation of the middle and C-terminal domains from yeast to humans suggests they are critical for decapping and proper mRNA decay, but how these domains interact with and activate mRNA decay factors remains unknown.

Here, we determine how Pat1 interacts with and activates both the Lsm1-7 complex and Dcp1/Dcp2 from the fission yeast *S.pombe (Sp)* using recombinant purified proteins, which recapitulate the regulation of decapping observed in budding yeast (Paquette et al. 2018; He and Jacobson 2015). We show that Pat1 promotes RNA binding of the Lsm1-7 complex using two short linear motifs from its middle domain that make physical interactions with the Lsm1-7 ring and enhance its interaction with RNA. Pat1 activates decapping using its middle domain and structured C-terminus, which directly binds conserved helical leucine motifs in Dcp2, to alleviate autoinhibition and promote substrate binding. Our results reveal how Pat1 nucleates assembly of a decapping mRNP and uses distinct domains to activate decay factors at both the 3' and 5' ends of a transcript to promote mRNA degradation.

Results

Pat1 makes bipartite interactions with Lsm1-7 to enhance RNA binding

Previous studies of Pat1 and Lsm1-7 purified from budding yeast indicate Pat1 is necessary to promote high affinity interactions with Lsm1-7 and RNA, and that the middle and C-terminal domains of Pat1 are sufficient to complement growth defects in strains where Pat1 is deleted (Pilkington and Parker 2008; Chowdhury et al. 2013). To understand the domains of Pat1 involved in mRNA turnover in S. *pombe*, we constructed strains harboring different domain deletions of Pat1(**Fig. 1.1A**). Both full length Pat1 and PatMC (residues 296-754) were sufficient to compliment the growth defect in the ΔPat1 strain. Neither the middle nor C-terminal domain alone, however, could rescue growth, which was not due to a protein expression defect (**Fig. 1.1B,C).** This suggests that, like budding yeast, both the middle and C-terminal domains of Pat1 are required for normal mRNA turnover in S.*pombe.*

To better understand how individual domains of Pat1 function in complex with Lsm1-7, we purified Maltose Binding Protein (MBP) fusions of different fission yeast Pat1 constructs and queried if they could enhance RNA binding of the Lsm1-7 complex. We used fluorescence polarization with an rA15 probe (termed oligoA), which mimics a deadenylated tail, to measure RNA binding and examined which regions of Pat1 could enhance the association of Lsm1-7 with RNA. Addition of MBP-PatMC enhanced the RNA binding of Lsm1-7, while PatC showed no effect (**Fig. 1.1D,E**). Importantly, PatMC alone bound oligoA RNA weakly, indicating the enhancement of RNA binding was due to enhancement of Lsm1-7 RNA binding.

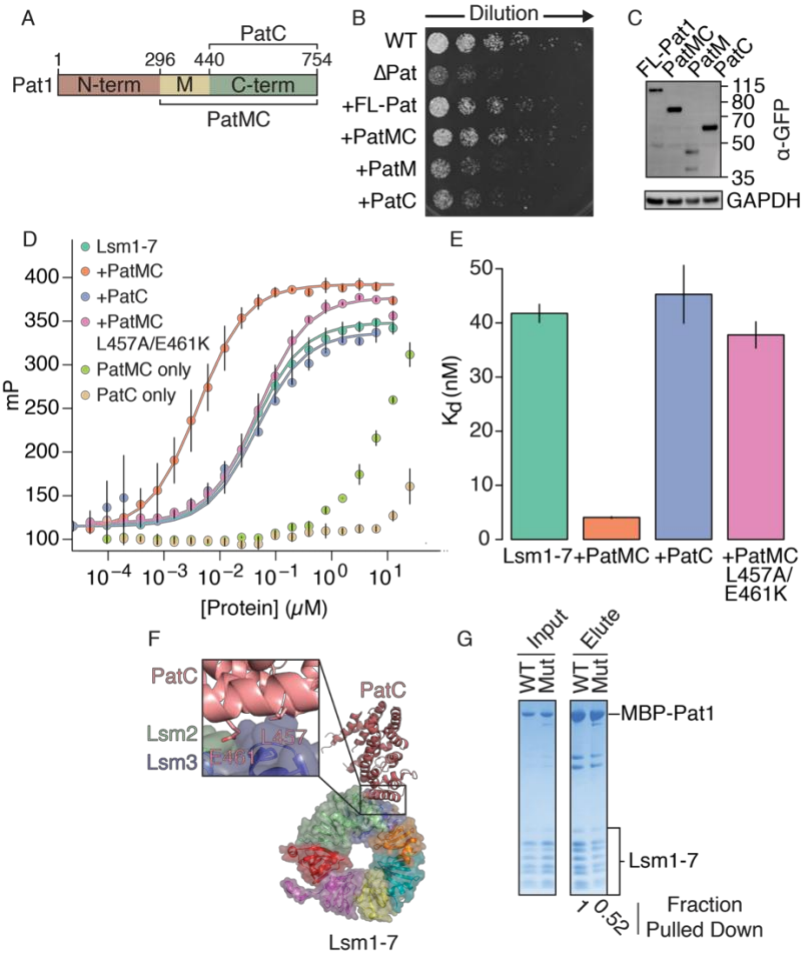

Figure 1.1: Pat1 makes a bipartite interaction with Lsm1-7 to enhance RNA binding
A, Schematic of Pat1 domains. **B,** Plate growth assay of S.*pombe* at 30 °C for ~1.5days with 4-fold dilutions from OD_{600} =0.115 on YES media. FL-Pat1 refers to full length Pat1. All proteins were expressed as C-terminal superfolderGFP fusions under control of the endogenous promoter and with the Ura4 3' UTR **C,** Western blot for expression of different Pat1 constructs detected with a GPF antibody and GAPDH as a loading control. Molecular weights in kDa are shown on right. **D,** Lsm1-7 binding 5' FAM-rA15 RNA (Lsm1-7, n=6; +PatMC, n=4, +PatC and +L457A/E461K, n=2) monitored by fluorescence polarization. All Pat1 constructs are N-terminal His_6MBP fusion proteins. **E,** Equilibrium dissociation constants determined from fits in **D** with standard deviation. **F,** Crystal structure of PatC interaction with Lsm1-7 (PDB 4C8Q) with magnification of PatC region contacting Lsm2 and Lsm3. Residues are numbered according to fission yeast and are conserved. **G,** MBP pull-down assay using 10 μM Lsm1-7 with stoichiometric amounts of MBP-Pat1 construct as input. Mut refers to the *Sp*PatMC L457A/E461K variant.

This effect was specific to oligoA, as Pat1 did not enhance binding to a U15 probe (**SI Appendix,**

Fig. S1.1A-C). To test if PatC's failure to enhance RNA binding of Lsm1-7 was simply due to an

inability to form a PatC/Lsm1-7 complex, we incubated PatC and Lsm1-7 together and were unable to observe a stable complex by analytical size exclusion chromatography (**SI Appendix, Fig. S1.2A,B**). This indicates that the PatC/Lsm1-7 interaction is likely weak and that the middle domain of Pat1 is required to enhance RNA binding of Lsm1-7 in part by promoting formation a stable heterooctameric complex.

Previous crystal structures have identified conserved residues on PatC that contact the Lsm2/3 subunits, and when mutated, lead to loss of complex formation and defects in mRNA degradation in budding yeast (**Fig. 1.1F**) (Wu et al. 2014; Sharif and Conti 2013). Introducing these mutations into *Sp*PatMC (L457A/E461K) minimally affected its association with Lsm1-7, as shown by pull-down analysis, but completely abrogated its ability to enhance Lsm1-7 RNA binding (**Figs. 1.1D,E,G**). This suggests that PatC must make specific interactions with Lsm2/3 to promote RNA binding and that the middle domain of Pat1 is required to form a stable complex with Lsm1-7. Furthermore, the inability of PatMC L457A/E461K to promote Lsm1-7 RNA binding suggests the middle domain is necessary, but not sufficient, to enhance function of the complex. We conclude that interactions of the middle and C-terminal domains of Pat1 with the Lsm1-7 ring are required to enhance RNA binding.

Short-linear motifs in the middle domain of Pat1 bind Lsm1-7 and enhance RNA binding

The middle domain of Pat1 could enhance RNA binding of Lsm1-7 by directly binding RNA, promoting a stable complex formation with Lsm1-7, or through both mechanisms. We first sought to identify which domain of Pat1 could associate with Lsm1-7. A construct containing most of the middle domain of Pat1, specifically residues 296-431, was necessary and sufficient to interact with Lsm1-7, while PatC was unable to form a stable complex by pull-down analysis (**Fig. 1.2)**.

This suggests the middle domain of Pat1 is responsible for promoting a stable complex with Lsm1-7.

We wanted to distinguish if the middle domain was only involved in protein-protein interactions or had additional roles in promoting RNA binding. To test these possibilities, we purified a series of N-terminal truncations of Pat1 and surveyed their ability to associate with Lsm1-7 by pull-down assays (**Fig. 1.2A,B,** truncations 1-4). Deletion of residues 296-431 abolished the Pat1/Lsm1-7 interaction, indicating that these residues are involved in associating with Lsm1-7 (truncation 3). This identifies residues in the middle domain of Pat1 that are required to form a stable complex with Lsm1-7.

Because we identified two N-terminal truncations of Pat1 that retained the ability to interact with Lsm1-7 to similar extent, we tested if these could enhance RNA binding of the PatMC/Lsm1-7 complex (**Fig. 1.2A,B**, truncations 1 and 2). If the sole function of the middle domain is to promote association with Lsm1-7, then all N-terminal truncations that interact with Lsm1-7 should enhance RNA binding. Contrary to this expectation, we found Pat1 317-754 was unable to stimulate RNA binding (**Fig. 1.2C,D**). This suggests that PatMC contains a region that is dispensable for PatMC/Lsm1-7 complex formation but essential for enhancing RNA binding. The binding isotherm for Pat1 317-754 is identical to the Lsm1-7/PatMC L457A/E461K mutant complex, which can also interact with Lsm1-7 but fails to enhance RNA binding (**Fig. 1.1B,C,E**). We therefore reason that residues 296-316 of Pat1 must be involved in stabilizing a productive complex that can bind RNA with high affinity, which we term the 'Lsm Activation Region' (LAR). The LAR is highly conserved in the *Schizosaccharomyces* genus, which is characteristic of short

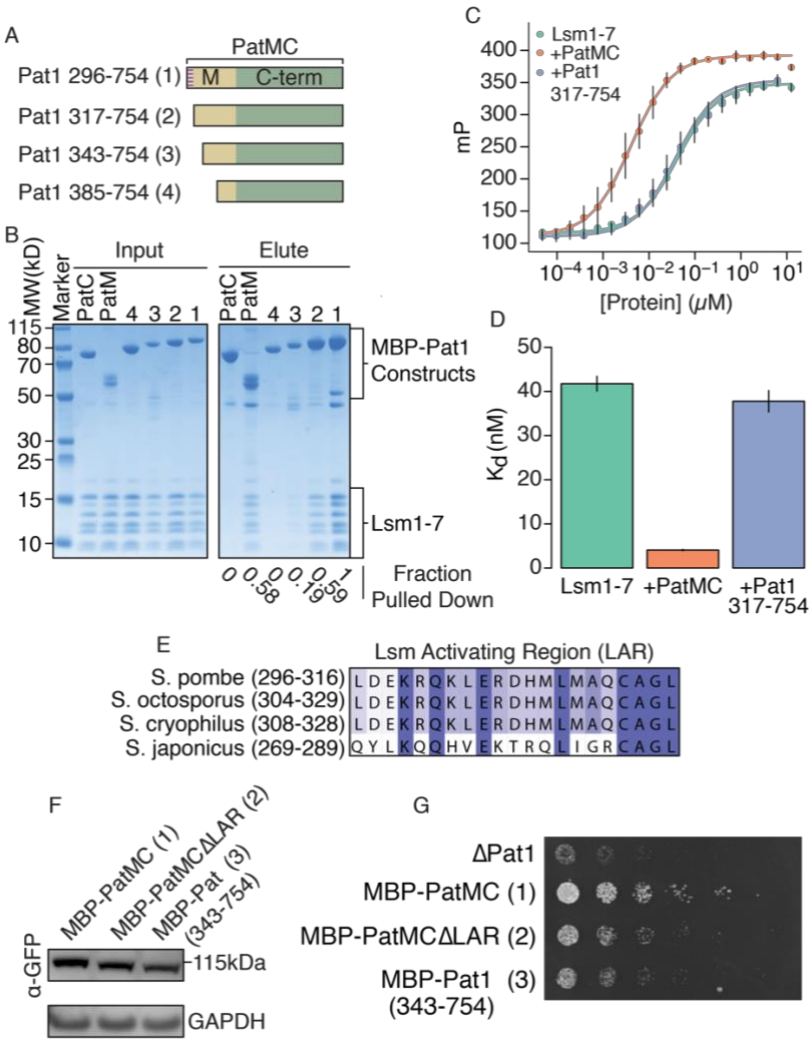

Figure 1.2: Separate regions of the middle domain of Pat1 interact with and enhance RNA binding by Lsm1-7

A, Schematic of different MBP-Pat1 constructs used in pulldown and binding assays. The Lsm Activation Region (LAR) is shown in stripes. **B,** Pulldown of 10μM Lsm1-7 with stoichiometric amounts of specified MBP-Pat1 construct. Numbers refer to schematic in **A**. **C,** Fluorescence polarization of 5' FAM-rA15 binding to reconstituted MBP-Pat1:Lsm1-7 complexes with standard deviation (Lsm1-7, n = 6; +MBP-PatMC; n=4, +MBP Pat1 317-754; n=4). All conditions contain stoichiometric amounts of Pat1/Lsm1-7. **D,** Dissociation constants of determined from fit to C with error bars representing standard deviation. **E,** Sequence alignment of the LAR in different *Schizosaccharomyces* species. **F,** Western blot for expression of different Pat1 constructs detected with a GPF antibody and GAPDH as a loading control. **G**, Plate growth assay of S.*pombe* at 30 °C for ~1.5days with 4-fold dilutions from OD_{600} =0.115 on YES media. All proteins were expressed as N-terminal MBP fusions to aid expression and C-terminal superfolderGFP fusions under control of the endogenous promoter and with the Ura4 3' UTR.

linear motifs that can be rapidly transferred between proteins during evolution (**Fig. 1.2E**) (Jonas and Izaurralde 2013). To understand the importance of the LAR for Pat1's function *in vivo*, we tested the ability of PatMC truncations to rescue cell growth. PatMC truncations were fused to an N-terminal MBP to permit expression (**Fig. 1.2F)**. Deletion of the LAR resulted in slow growth phenotype compared to PatMC alone. Additional truncation of Pat1 did not further reduce cell growth (**Fig. 1.2G**). Therefore, we conclude that the LAR of Pat1 is important for function in fission yeast. Metazoans have gained additional residues in this region, though we envision the LAR is still required for Lsm1-7 activation in higher order eukaryotes (**SI Appendix, Fig. S1.3**).

Our pulldown analysis and functional studies suggest that residues 317-342 in the middle domain of Pat1 are important for promoting a stable PatMC/Lsm1-7 complex. Sequence alignments reveal this region is conserved in Pat1 from yeast to humans (**Fig. 1.3A)**. To determine if this motif is necessary for the interaction of Pat1 with Lsm1-7, we constructed series of internal PatMC deletions by replacing intervening residues with a flexible $(GS)_3$ linker (**Fig. 1.3B**). Because appending the conserved motif containing amino acids 317-342 of the middle domain to PatC stabilized the interaction with Lsm1-7 (**Fig. 1.3C**), we refer to this region of Pat1 as the Lsm binding motif (LBM). In contrast, deletion of the LAR was dispensable for Pat1/Lsm1-7 interactions. While we cannot exclude that additional regions of Pat1 help stabilize the Pat1/Lsm1-7 complex, this data suggests the LBM helps mediate the protein-protein interaction with the Lsm1-7 ring. We conclude the middle domain of Pat1 contains two short linear motifs that may function separately in stabilizing the PatMC/Lsm1-7 complex and a conformation that is productive for RNA binding.

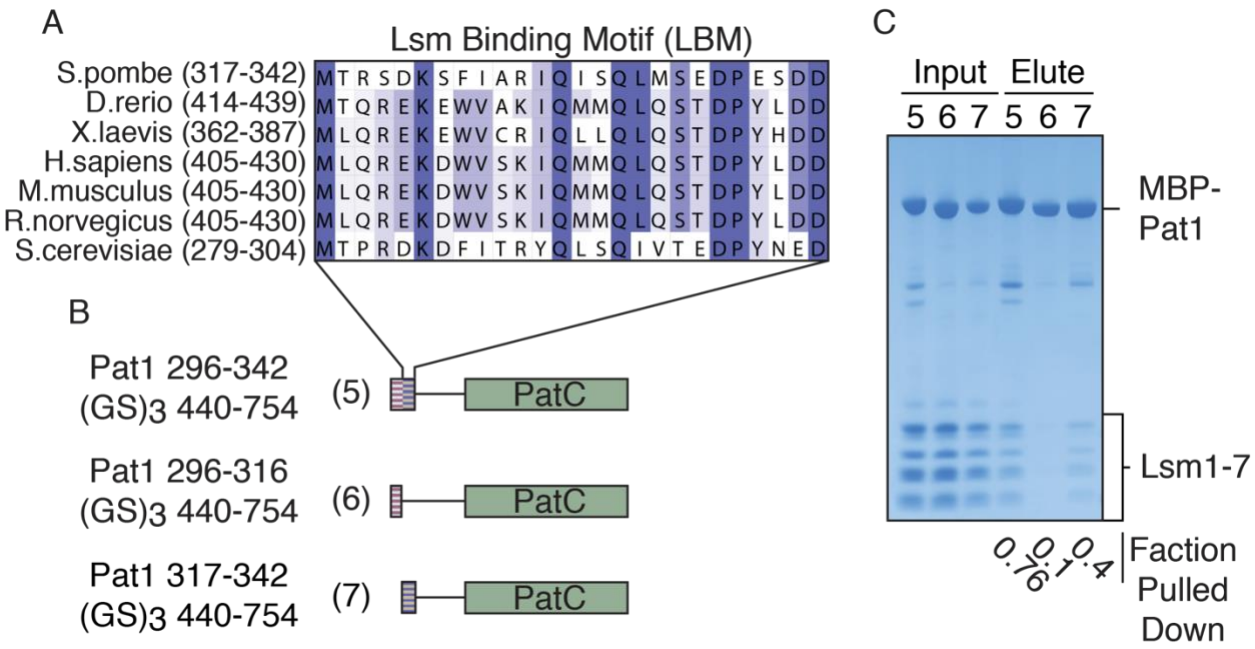

Figure 1.3: A short linear motif in the middle domain of Pat1 mediates protein-protein interaction with Lsm1-7
A, Conservation of the LBM in the Pat1 middle domain between different species. **B,** Schematic of constructs used. Residues were deleted and replaced with a flexible six amino acid $(GS)_3$ linker. The Lsm Activation Region (LAR) and Lsm Binding Motif (LBM) is shown in red or purple stripes, respectively. **C,** Pulldown of 10µM Lsm1-7 with stoichiometric amounts of MBP-PatMC internal deletions. Numbers refer to schematic in **A.**

The middle and C-terminal domains of Pat1 activate Dcp1/Dcp2

Numerous genetic experiments have demonstrated that the middle and C-terminal domains of Pat1 are required to enhance decapping *in vivo*, but the molecular mechanism has remained unclear (Pilkington and Parker 2008; Wu et al. 2014). Dcp2 contains a catalytic NUDIX hydrolase domain that cleaves the m7G cap, as well as a disordered C-terminal extension that is replete with regulatory elements such as inhibitory motifs and protein-protein interaction motifs. While we could not purify full length Dcp2, a C-terminally extended Dcp2 containing up to 261 additional amino acids recapitulates the regulatory elements in the full-length C-terminal extension (**Fig. 1.4A)** (Paquette et al. 2018; He and Jacobson 2015). The C-terminal domain of budding yeast Pat1 was crystallized with a helical leucine rich motif (HLM) of Dcp2, suggesting a mechanism by

which Pat1 could promote decapping (Charenton et al. 2017). Accordingly, we tested the ability of Pat1 to activate the decapping holoenzyme, Dcp1/Dcp2 *in vitro* using a C-terminally extended Dcp2 that contains two HLMs (Dcp1/Dcp2 1-318, termed Dcp1/Dcp2$^{HLM1/2}$) (**Fig. 1.4A**) (Wurm et al. 2016; Charenton et al. 2017). We chose this Dcp1/Dcp2 construct for initial studies to examine how Pat1 binding Dcp2 could function independent of inhibitory elements in the C-terminal extension of Dcp2. PatMC was able to enhance the activity of Dcp1/Dcp2$^{HLM1/2}$, while PatC had little effect on activity (**Fig. 1.4B**). This suggests that both the middle and C-terminal domain of Pat1 cooperate to directly activate decapping.

Although PatC was unable to stimulate decapping on its own, we next asked if it could directly associate with HLMs of Dcp2 using ^{15}N HSQC NMR spectroscopy. We purified ^{15}N labelled Dcp2 containing a single HLM (Dcp2 1-266, termed Dcp2-HLM1, **Fig. 1.4A**), and determined if any chemical shift perturbations (CSPs) occurred in the presence of PatC. Upon addition of PatC, we observed losses and reappearances of resonances in Dcp2-HLM1 but not in the Dcp2 catalytic core alone (Dcp2 1-243, termed Dcp2^{Core}) (**Fig. 1.4D & SI Appendix, Fig. S1.4**). This indicates that PatC directly binds HLMs in Dcp2. Furthermore, HLM-1 of Dcp2 was sufficient for binding PatC, assayed by NMR CSP analysis and copurification by size-exclusion chromatography (**Fig. 1.4E & SI Appendix, Fig. S1.5A-D**). We conclude that fission yeast PatC is sufficient to interact with Dcp2 by binding HLMs, but both the middle and C-terminal domains are required to activate decapping (Charenton et al. 2017).

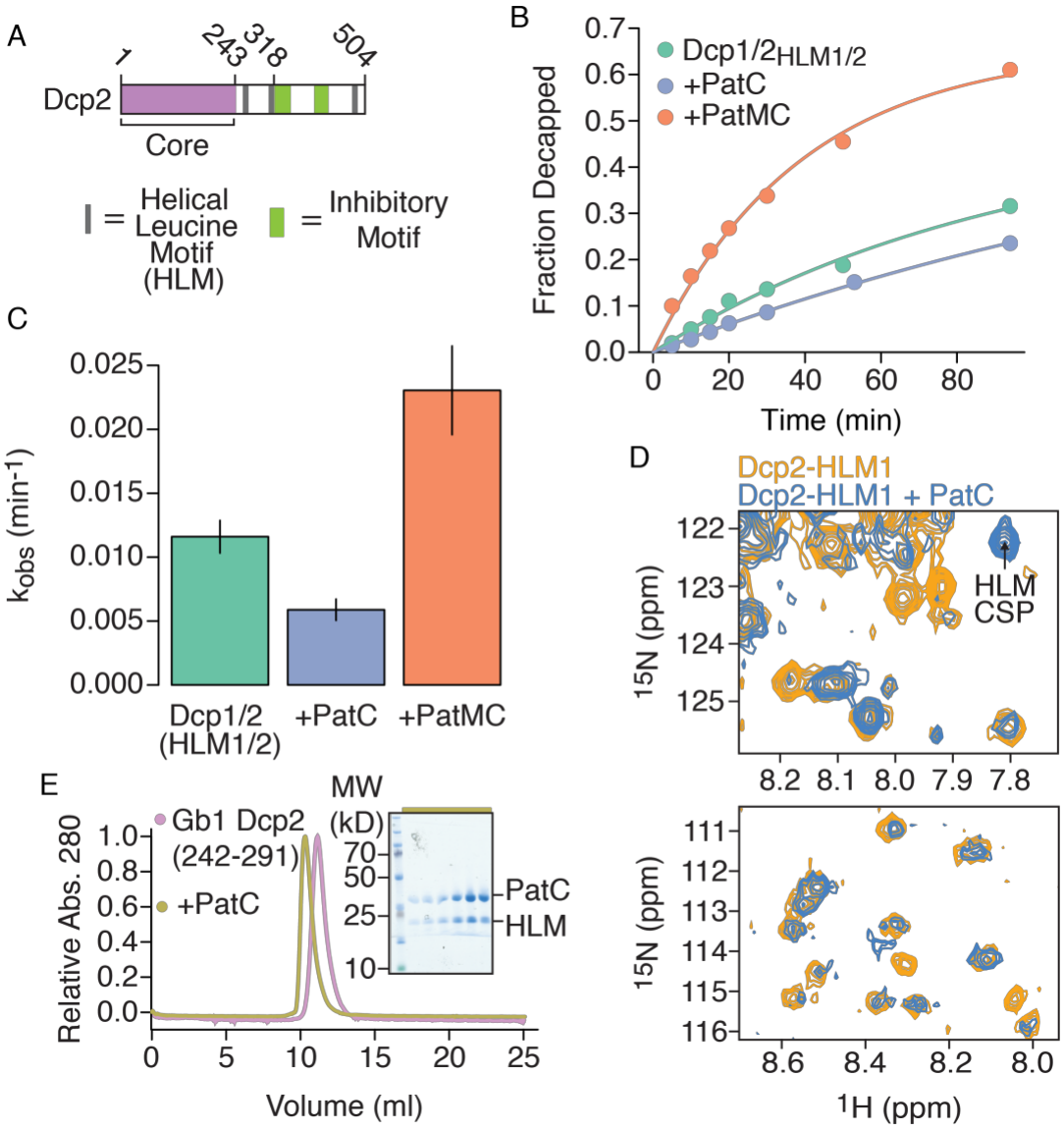

Figure 1.4: Pat1 directly binds and activates C-terminally extended Dcp2 constructs
A, Schematic of domains of Dcp2. The structured core that hydrolyzes cap is shown in purple. Gray boxes represent helical leucine motifs and green boxes represent inhibitory elements. **B,** Representative decapping of an RNA with 150nM Dcp1/Dcp2$_{HLM1/2}$ and 10µM of MBP-tagged Pat1 construct. **C,** Rates determined from **B** displayed with standard deviation (n=2). **D,** Magnified views of regions of interest in ^{15}N-^{1}H HSQC of 100µM Dcp2$_{HLM1}$ with or without 150µM PatC. Full spectrum is in SI Appendix, Fig. S1. **E,** Analytical size exclusion chromatography of 35µM H$_6$-GB1-Dcp2 242-291 alone (pink) or with a stoichiometric amount of PatC (gold). Insert is gel corresponding to peak in gold trace. The helical leucine motif sequence is residues 257-264 of Dcp2.

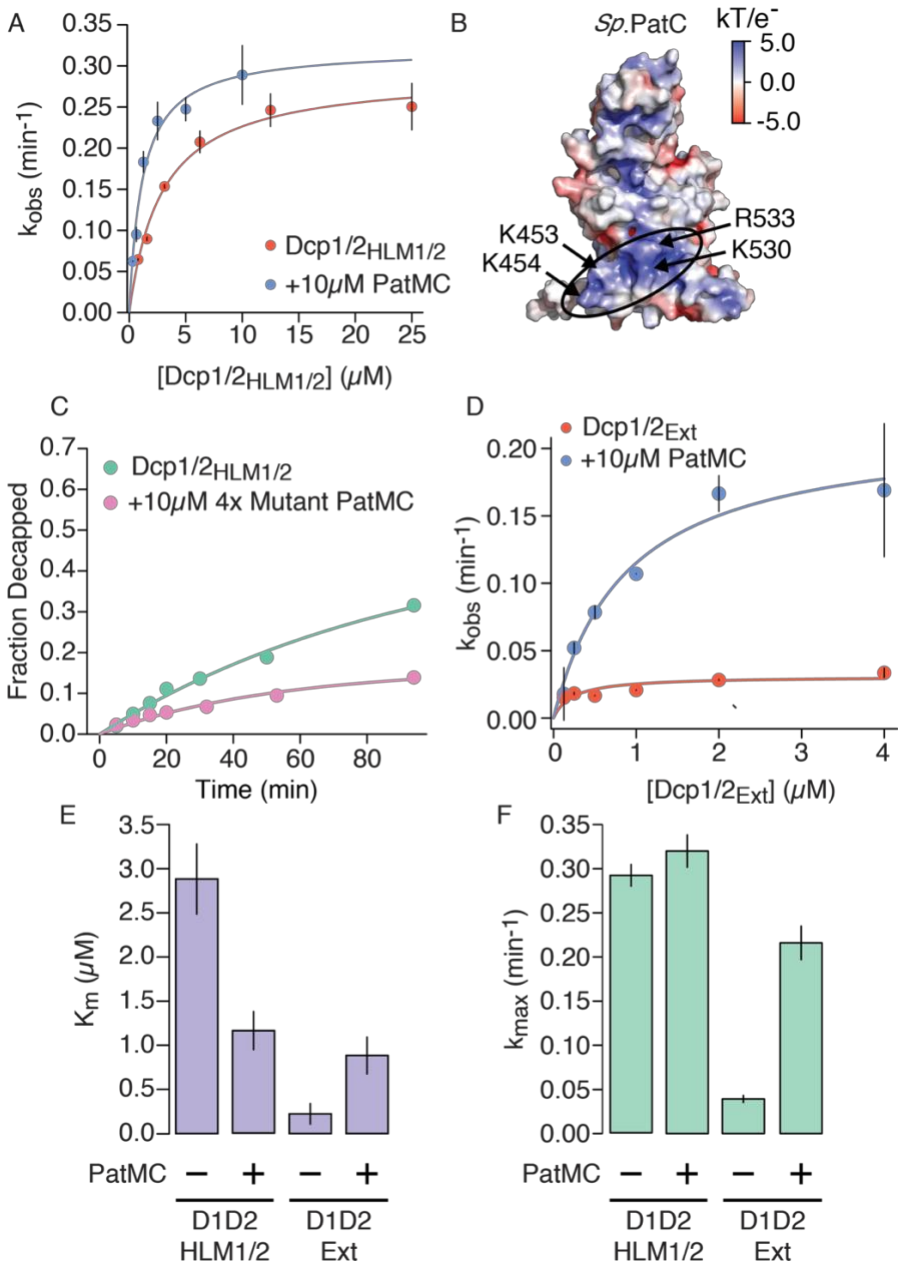

Figure 1.5: The middle domain differentially activates C-terminally extended Dcp2 constructs

A, Single-turnover kinetic analyses of Dcp1/Dcp2$_{HLM1/2}$ alone or in the presence of 10μM MBP-PatMC (n=2)**. B,** Electrostatic surface representation of model of *Sp*PatC based on PDB 5LMG using modeler (Eswar et al. 2006) and APBS in pymol (Schrödinger). Basic patch is circled, while residues mutated are indicated with arrows. **C,** Representative decapping assay of an RNA with 150nM Dcp1/Dcp2$_{HLM1/2}$ and 10μM 4x mutant MBP-PatMC (K453A/K454A/K530A/R533A). **D,** Single-turnover kinetic analyses of autoinhibited Dcp1/Dcp2$_{Ext}$ alone or in the presence of 10μM MBP-PatMC (n=2). **E-F,** K_M and k_{max} values calculated from **A** and **D** for Dcp1/Dcp2$_{HLM1/2}$ or Dcp1/Dcp2$_{Ext}$ alone or in the presence of 10μM MBP-PatMC shown with standard deviation**.**

To gain insight into how Pat1 activates decapping by Dcp1/Dcp2 in the absence of inhibitory elements, we determined the kinetic parameters of Dcp1/Dcp2$_{HLM1/2}$ either alone or in the presence of MBP-PatMC using a single turnover decapping assay (**Fig. 1.5A**). We used saturating PatMC in all experiments to ensure complete formation of a PatMC/Dcp1/Dcp2 complex at all measured concentrations. While we observed minimal effects on k_{max}, we saw a ~3-fold reduction in K_m (**Fig. 1.5E-F**). This suggests that PatMC can bind to HLMs in Dcp2 to enhance substrate binding of the decapping complex.

While *Sp*PatC had no effect on decapping *in vitro*, we hypothesized that, like the Lsm1-7 complex, both the middle domain and C-terminal domains of Pat1 may cooperate to enhance the activity of Dcp1/Dcp2. Studies of human PatC identified a basic patch that is required for mRNA decapping and decay (Braun et al. 2010). Modeling of *Sp*PatC onto existing crystal structures reveals a similar basic patch to that identified in humans, which we reasoned may be involved in activating Dcp2 (**Fig. 1.5B**). Mutation of these four basic residues to alanine (K453A/K454A/K530A/R533A, referred to as 4x Mutant) in *Sp*PatMC abolished its ability to activate Dcp1/Dcp2 (**Fig. 5C**). Because the middle domain and residues on the C-terminal domain of Pat1 are both required to activate decapping, these domains may form a bipartite RNA-binding surface that can recruit Dcp1/Dcp2 to substrate. This suggests that PatC can bind HLMs and cooperate with the middle domain of Pat1 to increase the affinity of Dcp1/Dcp2 for substrate RNA.

In addition to HLMs, the C-terminal region of Dcp2 contains inhibitory elements that promote nonproductive binding of Dcp1/Dcp2 to substrate to limit catalysis (**Fig. 1.4A**). Other HLM

binding proteins, such as Edc3, have been shown to relieve autoinhibition (Paquette et al. 2018). To interrogate how PatMC activates an autoinhibited Dcp1/Dcp2, we determined the kinetic parameters of an extended Dcp1/Dcp2 construct that contains both inhibitory elements and HLMs (Dcp1/Dcp2 1-504, termed Dcp1/Dcp2$_{Ext}$), either alone or with saturating amounts of PatMC. Unlike the Dcp1/Dcp2$_{HLM1/2}$, PatMC activated the catalytic step of decapping, while also decreasing the affinity of Dcp1/Dcp2$_{Ext}$ for substrate (**Fig. 1.5A, C-D**). This suggests that Dcp1/Dcp2$_{Ext}$ binds nonproductively to RNA, and PatMC activates catalysis at the expense of substrate binding. This is in agreement with HLM binding proteins relieving autoinhibition to promote decapping, suggesting this may be a general model for proteins that bind the C-terminus of Dcp2. We conclude Pat1 uses its middle and C-terminal domains to alleviate autoinhibition and enhance substrate binding of the Dcp1/Dcp2 decapping enzyme complex.

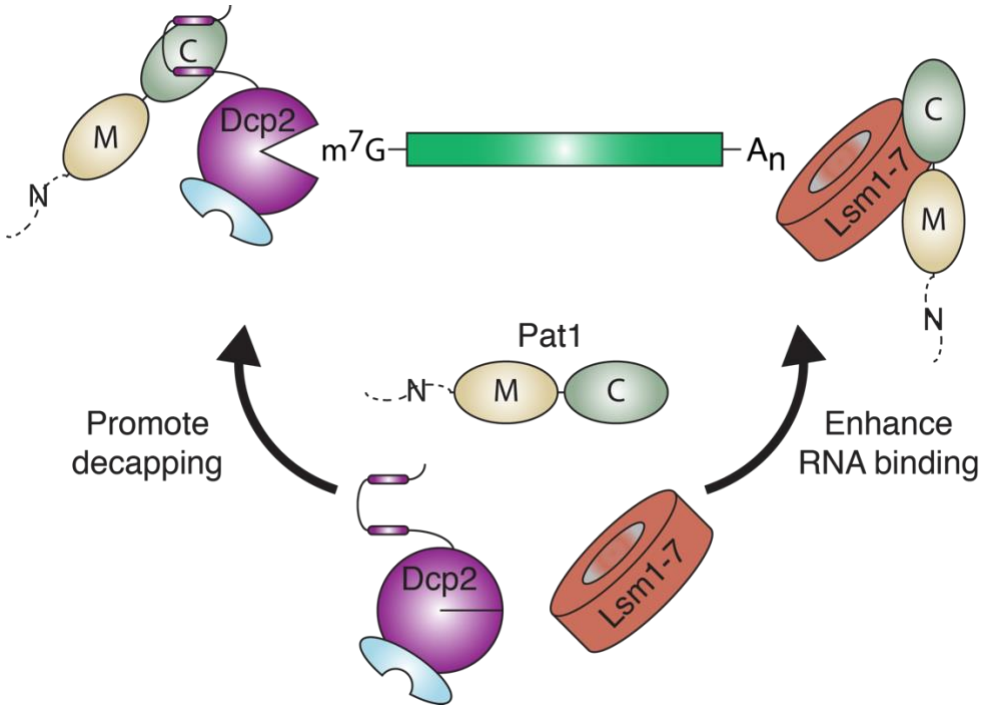

Figure 1.6: Model for how Pat1 interacts with and activates multiple RNA decay factors to establish 5' decapping
Pat1 interacts with and activates decay factors at both the 5' and 3' ends of the mRNA to promote decapping.

Discussion

Pat1 works together with Dcp1/Dcp2 and the Lsm1-7 complex to promote bulk 5'-3' decay on numerous transcripts in yeast (He et al. 2018). Our work reveals how Pat1 interacts with and activates separate steps in this pathway. First Pat1 enhances the RNA binding of Lsm1-7 complex using a bipartite interaction surface comprised of its middle and C-terminal domain. Second, Pat1 promotes decapping by Dcp1/Dcp2 using both domains to affect RNA binding and alleviate autoinhibition. Taken together, these results provide a mechanistic framework for how Pat1 can enhance binding and activity of factors that act on the 5' and 3' ends of mRNA to promote bulk decay (**Fig. 1.6)**.

Pat1 enhances binding of the Lsm1-7 complex to oligoA RNA 10-fold using bipartite interactions of its middle and C-terminal domains (**Fig. 1.1**). This requires short-linear motifs within the middle domain of Pat1, termed the Lsm binding motif (LBM) and Lsm activating region (LAR), that mediate complex formation with Lsm1-7 and enhance oligoA binding (**Figs. 1.2 & 1.3**). Interactions of the C-terminal domain of Pat1 with Lsm2/3, as predicted by crystallographic analyses, are necessary for assembly of a stable complex between Pat1, the Lsm1-7 ring and RNA. Pat1 constructs lacking the Lsm activating region (LAR) still interact with Lsm1-7 but fail to enhance RNA binding. Therefore, protein interactions required for formation of a stable Pat1 and Lsm1-7 complex can be separated from the ability of Pat1 to enhance RNA binding of Lsm1-7. The middle domain has a role beyond the promoting the interaction between Pat1 and Lsm1-7 and is likely involved in stabilizing a conformation of Lsm1-7 that can bind RNA with high affinity. The molecular details of how the middle domain of Pat1 interacts with the Lsm1-7 ring and enhances RNA binding will require high-resolution structural studies.

The mechanism by which the Pat1/Lsm1-7 complex recognizes and targets mRNAs for decapping remains poorly understood. In budding yeast, Pat1/Lsm1 bind the 3' end of mRNAs and promotes degradation of inefficiently translated transcripts. Furthermore, biochemical evidence suggests preferential binding of deadenylated, oligoA tails (Mitchell et al. 2012; He et al. 2018; Chowdhury et al. 2007). In S.*pombe* and higher order eukaryotes, however, an additional 1-3 uridines are added to a subset of transcripts after deadenylation but prior to decapping, which are enriched when Lsm1 is deleted (Rissland and Norbury 2009; Lim et al. 2014). Understanding how different mRNA tail modifications affect Pat1/Lsm1-7 recognition in cells remains a challenge for the future.

Multiple decapping activators bind the C-terminal regulatory region of Dcp2 to activate decapping and ensure transcript specificity in cells. We show that Pat1 directly activates decapping by binding helical leucine rich motifs (HLMs) in the C-terminal regulatory region to enhance Dcp1/Dcp2 RNA binding and alleviate autoinhibition (**Figs. 1.4-5**). This mechanism is reminiscent of other HLM binding proteins, such as Edc3, and may be a general mechanism by which HLM binding proteins promote decapping. Importantly the middle domain and structured C-terminus are both required for these effects. This is consistent with early work showing the middle domain is required to activate decapping in yeast and recent structural work showing C-terminal domain binds Dcp2 (He and Jacobson 2015; Charenton et al. 2017). Taken with our biochemical characterization of the Pat1/Lsm1-7 interaction, these observations suggest that both the middle and C-terminal domains of Pat1 are required to activate distinct steps of mRNA decay. It is likely that deletion of the middle domain has a strong defect in decapping because of reduced Lsm1-7 RNA binding and activity of Dcp1/Dcp2 on substrate mRNA.

Previous studies from budding yeast, flies, and humans have demonstrated that Pat1 interacts with multiple decay factors and is required for normal mRNA turnover *in vivo,* which requires both the unstructured middle domain and globular C-terminal domain. In humans, PatC can interact with Lsm1-7, while in flies, the middle domain is sufficient for association (Braun et al. 2010; Haas et al. 2010). Budding yeast PatC can interact with Lsm1-7, but requires cooperation between both the middle and C-terminal domains to promote RNA binding (Wu et al. 2014; Sharif and Conti 2013; Chowdhury et al. 2013). Both the middle and C-terminal domains in flies can interact with Dcp2, though in humans and budding yeast, the C-terminal domain of Pat1 is sufficient (Braun et al. 2010; Charenton et al. 2017; He and Jacobson 2015; Nissan et al. 2010; Haas et al. 2010). It is clear that the relative strengths of the interactions between Pat1 and different RNA decay factors has changed during the course of evolution, which may a potential mode of regulation for the assembly of RNA decay factors. Our biochemically reconstituted system defines how short-linear motifs in the disordered middle domain with the structured C-terminal domain cooperate to promote distinct steps during 5'-3' mRNA degradation.

Our work demonstrates how conserved short-linear motifs of the unstructured middle domain of *Sp*Pat1 enhance Lsm1-7, which may be applicable to nuclear Lsm2-8 complexes. Recent genome-wide analysis of the vertebrate orthologue of Pat1 (Pat1b/PatL1) suggest it functions with the Lsm2-8 complex during pre-mRNA splicing in addition to its established role with Lsm1-7 in mRNA decay. Ablation of Pat1b promotes skipping of exons with weak donor site sequences, in addition to increasing the steady-state levels of AU rich containing mRNAs. Knockdown of Pat1b reduces formation of the U6 snRNP containing Lsm2-8 and SART3 (an orthologue of yeast Prp24). Furthermore, Pat1b is localized in nuclear Cajal bodies as well as cytoplasmic processing

bodies (Vindry et al. 2017). The unstructured middle domain of Pat1 may endow it with structural plasticity, allowing it to function as a versatile chaperone for RNP assembly during bulk 5'-3' mRNA decay and pre-mRNA splicing.

Materials and Methods

RNA transcription and capping

A 340 nucleotide RNA containing a short oligo A tail of 15 nucleotides and corresponding to the MFA2 gene of budding yeast was *in vitro* transcribed and capped according to previous protocols (Jones et al. 2008). Briefly, RNA was transcribed using T7 RNA polymerase and purified on a 6% denaturing polyacrylamide gel. RNA was excised from gel and extracted before being further purified by phenol:chloroform and ethanol precipitation. RNA was capped with α-^{32}P GTP using vaccinia virus capping enzyme and separated by gel purification, phenol:chloroform extraction and ethanol precipitation as previously described (Jones et al. 2008).

Decapping Kinetics

Decapping assays with Dcp1/Dcp2 and cofactors were performed at room temperature in a buffer containing 150mM NaCl, 20mM HEPES pH = 7, 1mM DTT, 5mM $MgCl_2$ with 0.3μg/μl Acetylated Bovine Serum Albumin. Reactions were performed under single-turnover conditions, where enzyme (Dcp1/Dcp2) is in excess over substrate. The concentration of MBP-Pat1 constructs was 10 μM MBP-Pat1 in all experiments. Proteins were mixed at desired concentrations and incubated at room temperature for 30 minutes before initiating the reaction with ^{32}P capped-RNA. Time points were taken and quenched in 0.5 M EDTA before being analyzed by Thin Layer Chromatography. Data were phosphoimaged with a Typhoon scanner (GE) and analyzed using ImageQuant software (GE). Rates were obtained by fitting to a first-order exponential or, when

applicable, a linear model. Kinetic constants were obtained by increasing Dcp1/Dcp2 concentrations and time-courses as previously described (Jones et al. 2008).

Fluorescence Polarization

Fluorescence polarization was performed in 384-well low volume plates (Greiner) in the same buffer used for decapping kinetics. Oligo RNAs with 5' FAM were ordered from IDT and used at a final concentration of 500 pM. To assemble Pat1/Lsm1-7 complexes, stoichiometric amounts of the Pat1 construct and Lsm1-7 were mixed together on ice for 10 minutes prior to setting up reaction. Reactions were incubated for five minutes before measuring polarization on an Analyst AD plate reader (LJL Biosystems). Equilibrium dissociation constants (K_d) were fit to the equation for oligo A15:

$$Y(mp) = (\max(mp) - \min(mp)) * \frac{[protein]}{[protein] + K_d} + \min(mp)$$

or for U15, when probe concentration was close to K_d

$$Y(mp) = ((\max(mp) - \min(mp)) * \frac{([protein]^n + {k_d}^n + [probe]^n)^2 - \sqrt{([protein]^n + {k_d}^n + [probe]^n)^2 - 4[protein]^n[probe]^n}}{2[probe]^n} + \min(mp)$$

where n represents the Hill coefficient. Plots and fits were generated using in house scripts written in R, which are available at https://github.com/jhlobel/FP-fitting.

Cloning and Protein Purification

All seven Lsm genes were codon optimized for expression in *E.*coli and synthesized as polycistronic gene (IDT). The genes were in order from Lsm1 to Lsm7, where each gene was

separated by a 28nucleotide spacer followed by a ribosome binding site. The polycistron was cloned into a vector with an His_6-TEV site on the N-terminus of Lsm1. Unless stated otherwise, proteins were expressed in BL21(DE3)-Star cells in LB media. Cells were grown to OD_{600}=0.6 at 37 °C. IPTG was added to 1 mM and cells were grown shaking overnight at 17 °C. Cell pellets were harvested by centrifugation and lysed in appropriate buffer. For Lsm1-7, cells were lysed in Buffer A (2 M NaCl, 20 mM HEPES, 20 mM Imidazole, 5 mM βME, protease inhibitor, lysozyme, pH=7.5) by sonication. Lysate was subsequently clarified by centrifugation and the supernatant was bound to Ni-NTA resin at 4 °C for 1 hour. The resin was then loaded into a gravity column and washed with 20 column volumes of Buffer A. All proteins were eluted in Buffer E (250 mM NaCl, 250 mM Imidazole, 20 mM HEPES, 10 mM βME) and tags were cleaved with TEV protease overnight at 4 °C before being loaded onto a HiTrap Heparin column (GE). The heparin column was run at 2 ml/min from a 0.25-1 M NaCl gradient over 20 column volumes. Fractions containing protein complex were collected and further purified by gel filtration using a Superdex 200 16/60 column (GE) equilibrated in SEC buffer (20 mM HEPES pH =7, 150 mM NaCl, 1 mM DTT). Fractions containing protein were concentrated before being flash frozen and stored at -80 °C.

For expression of GB1-HLM1 (residues 242 to 291 of *Sp*Dcp2) and MBP-Pat1 constructs, cells were lysed in Buffer B (500 mM NaCl, 20 mM Imidazole, 5 mM βME, 20 mM HEPES pH = 7) and bound to nickel resin before being washed with 20 column volumes of Buffer B. Protein was then eluted in with Buffer E, and if necessary, tags were TEV cleaved overnight. We found the MBP tag to be essential for purification of all Pat1 constructs that contained the middle domain, so it was not removed. Elutants were concentrated and further purified by S200 16/60 in SEC buffer. Peak fractions were pooled and concentrated before being flash frozen.

Dcp1/Dcp2$_{HLM1/2}$ or Dcp1/Dcp2$_{Ext}$ was coexpressed and purified by Ni-NTA chromatography as described for MBP-Pat1 except with an additional purification step. After elution from Ni-NTA resin, TEV was added and the protein was cleaved overnight before being loaded onto Streptactin resin (IBA). The column was washed with 20 column volumes of Buffer B and eluted in Buffer B supplemented with 10 mM desthiobiotin. The elution was the concentrated and purified on an S200 16/60 in SEC buffer. Sodium Chloride was added to 300 mM before being concentrated and flash frozen.

Copurification by Analytical Size Exclusion Chromatography

Samples were mixed at ~35μM in 500μl volume before being filtered and injected onto a GE Superdex 75 10/300. All samples were run in 20mM HEPES pH =7.5, 1mM DTT with either 400 mM NaCl for Lsm1-7+PatC or 150 mM NaCl for PatC+GB1 Dcp2 242-291. Samples were run at 0.35ml/min and peaks were analyzed by SDS-PAGE (Invitrogen).

NMR

^{15}N labelled GB1 Dcp2 242-291 (HLM1), Dcp2 1-243 (Dcp2$_{core}$), and Dcp2 1-266 (Dcp2-HLM1) were expressed in H_2O-based minimal media with $^{15}NH_4Cl$ as the sole nitrogen source. For ^{13}C ILV labelling of GB1-Dcp2 242-291 precursors were added (Ile: 50mg/L, Leu/Val: 100mg/L) 40minutes prior to induction. IPTG was added to 1mM and proteins were expressed overnight at 18 °C. Cells were lysed in Buffer B and purified by on Ni-NTA resin. For Dcp2 constructs, the tag was cleaved by addition of TEV. Proteins were then purified by size-exclusion chromatography on a superdex 75 16/60 in NMR buffer (21 mM NaH_2PO_4, 28.8 mM Na_2PO_4, 200 mM NaCL, 100 mM Na_2SO_4, 5mM DTT). All ^{1}H-^{15}N and ^{1}H-^{13}C HSQC experiments with PatC and Dcp2 were

performed with 100 µM Dcp2 and 150 µM PatC in NMR buffer and recorded at 303 K on a Bruker Avance 800 spectrometer equipped with a cryogenic probe.

Pull downs

All pulldowns were done in SEC buffer. Briefly, 10µM of MBP-tagged Pat1 construct and 10µM Lsm1-7 were mixed and incubated at room temperature for 15 minutes before being added to pre-equilibrated amylose beads (New England Biolabs) for 5 minutes. The beads were spun down at 4000g for 2 minutes and samples were washed four times with 500 µl SEC buffer before being eluted with 30 µl SEC buffer supplemented with 10 mM Maltose. Eluted samples were resolved on 4-12% Bis-Tris SDS-PAGE gel (Invitrogen) and stained with Instant Blue (Expedeon). All input was loaded diluted 8-fold compared with elution to account for unbound Pat1/Lsm1-7 constructs. Fraction pulldown was calculated from the following equation:

$$Fraction\ Pulled\ Down = \frac{\frac{I_{Lsm1}}{I_{Lsm1} + I_{Pat\_Construct}}}{\frac{I_{Lsm1}}{I_{Lsm1} + I_{PatMC}}}$$

, where I_{lsm1} and I_{PatMC} are the intensities of the background subtracted Lsm1 and PatMC intensities, respectively. $I_{Pat\_Construct}$ is the intensity of the specified Pat1 construct. This equation normalizes all pulldowns to PatMC/Lsm1-7. All intensities were obtained by quantifying the same size area in ImageJ and background subtracted. Lanes that had Lsm1 intensities below background were adjusted to zero. We chose to quantify only Lsm1 band, as commassie staining is nonlinear and decreases with the molecular weight of the protein.

Fission yeast strain construction and growth assays

All strains were constructed by knocking in C-terminally tagged superfolderGFP Pat1 constructs into the commercially available pat1::KanMX background (Bioneer). A list of strains used in this study are provided in **Table S1**. All Pat1 constructs were cloned with a C-terminal superfolderGFP tag and Ura4 3' UTR and cloned into a pUC-19 vector containing 500 basepairs upstream and downstream of the Pat1 locus with a Hygromycin resistance cassette (Al-sady et al. 2016). Plasmids were linearized with restriction enzymes and knocked into appropriate yeast strains by either LiOAc transformation or electroporation (Forsburg and Rhind 2006). To verify knock in at the correct genomic locus DNA was obtained by phenol:cholorom extraction and tested for presence of correct genomic insertion by PCR. Colonies containing the knock in at the correct locus were stored as glycerol stocks at -80 ºC. For plate growth assays, yeast strains were grown overnight in YES and diluted to OD_{600} = 0.115 and serially diluted 4-fold before being spotted onto YES plates and grown for ~1.5 days at 30 ºC.

For western blots, cells were grown overnight and diluted to OD_{600} = 1 the following day. Cells were pelleted by centrifugation and protein was extracted with 2M NaOH/10mM BME supplemented with a protease inhibitor tablet (Roche). 55% Trichloroacetic acid was then added to precipitate protein, and then centrifuged at 16,000rpm for 20 minutes at 4 ºC. The supernatant was removed and the pellet was resuspended in HUE buffer (8M Urea, 1%SDS, 50mM EDTA, 10mM BME) and heated to 70 ºC for 15 minutes before flash freezing and storing at -80 ºC. Western blots for protein expression were performed using antibodies against GFP and GAPDH as a loading control (Proteintech) and detected with StarBright™ 700 goat anti-mouse IgG (Biorad) on a ChemiDoc (Biorad) using the Qdot705 channel.

Supplemental Figures

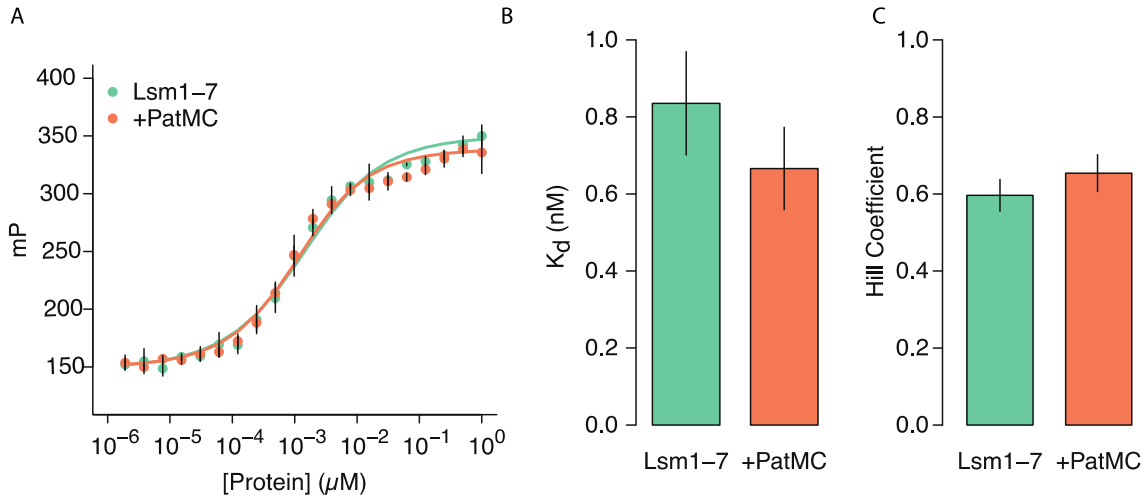

Supplemental Figure 1.1: PatMC does not enhance RNA binding for U15
A, Lsm1-7 binding 5' FAM-U15 RNA alone or with H_6MBP-PatMC (both n=3) monitored by fluorescence polarization. The data was fit to a quadradic binding equation with cooperativity. **B,** Dissociation values from **A** with standard deviations. **C,** Hill coefficients from **A** with standard deviations.

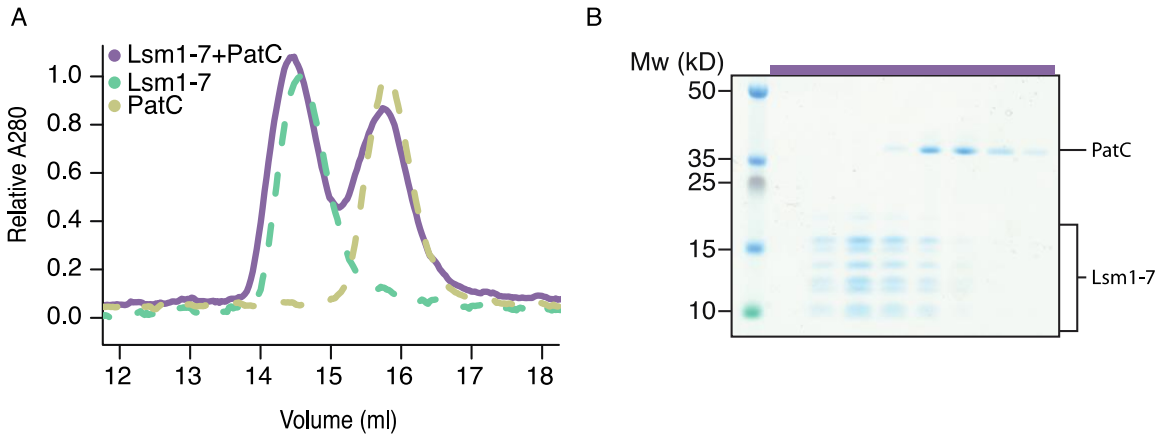

Supplemental Figure 1.2: PatC does not stably interact with Lsm1-7
A, Analytical size exclusion chromatography of PatC, Lsm1-7, or combined PatC/Lsm1-7. All proteins were at ~25μM and run in a 400mM NaCl buffer. **B**, Gel corresponding to fractions of Lsm1-7 + PatC SEC in Figure 3C. The purple bar on top corresponds to purple chromatogram.

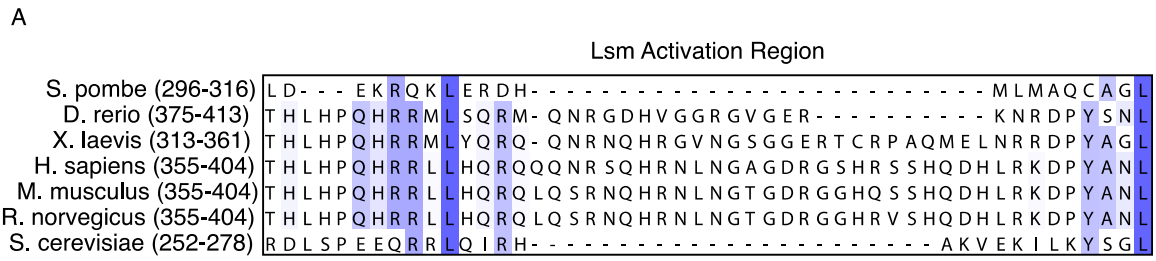

Supplemental Figure 1.3: Sequence alignments of the Lsm Activation Region (LAR).
A, Sequence alignment of different species of the LAR. Metazoans have acquired additional residues that may be functionally important for enhancing the RNA binding of Lsm1-7.

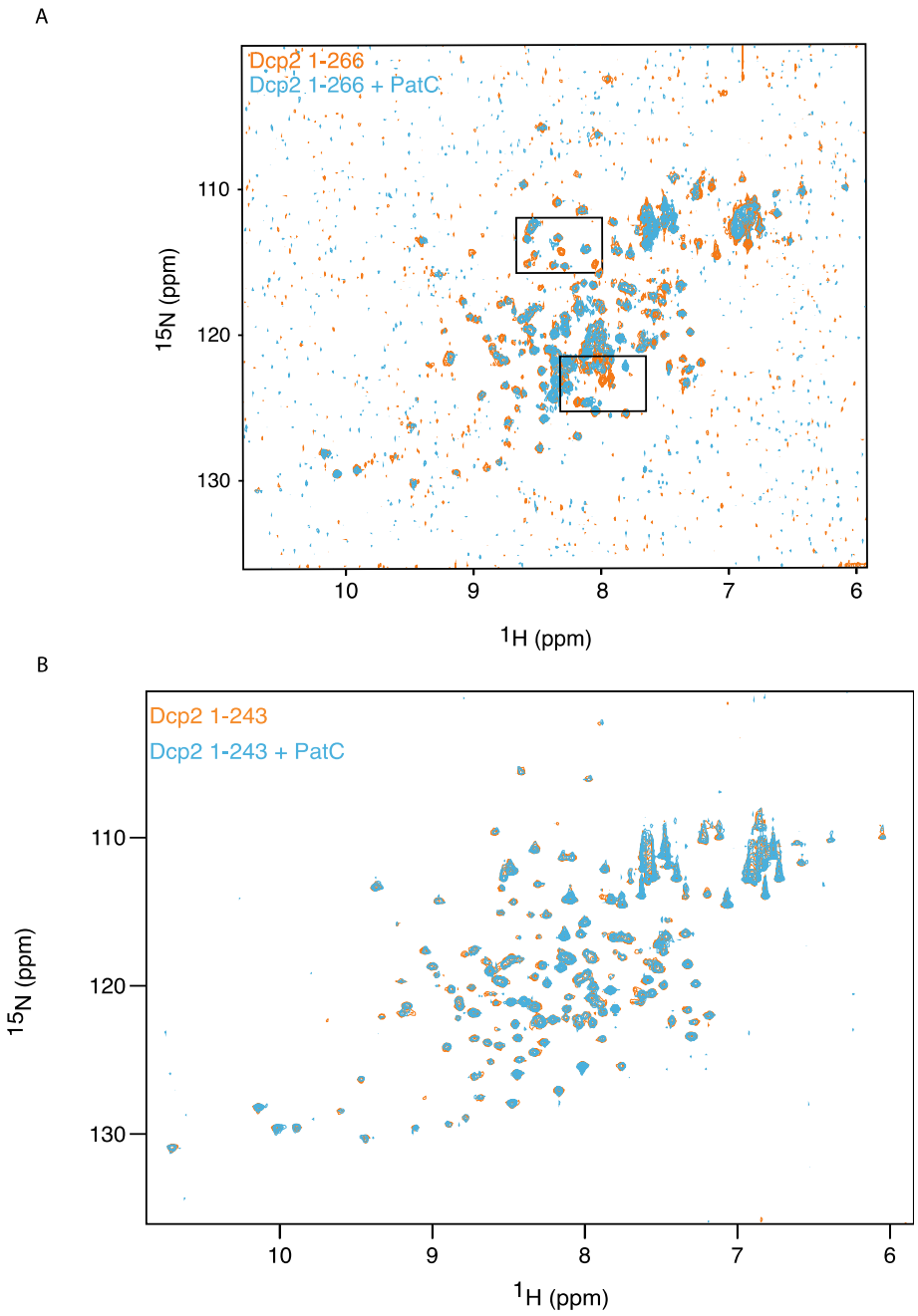

Supplemental Figure 1.4: Full 15N-1H HSQC of Dcp2 constructs ± PatC

A, Full spectrum of 100µM ^{15}N labeled Dcp2^{HLM1} in the presence or absence of 150µM PatC. Boxes represent magnified views shown in Figure 1D. **B**, ^{15}N-^{1}H HSQC of 100µM Dcp2^{Core} with or without 150µM PatC.

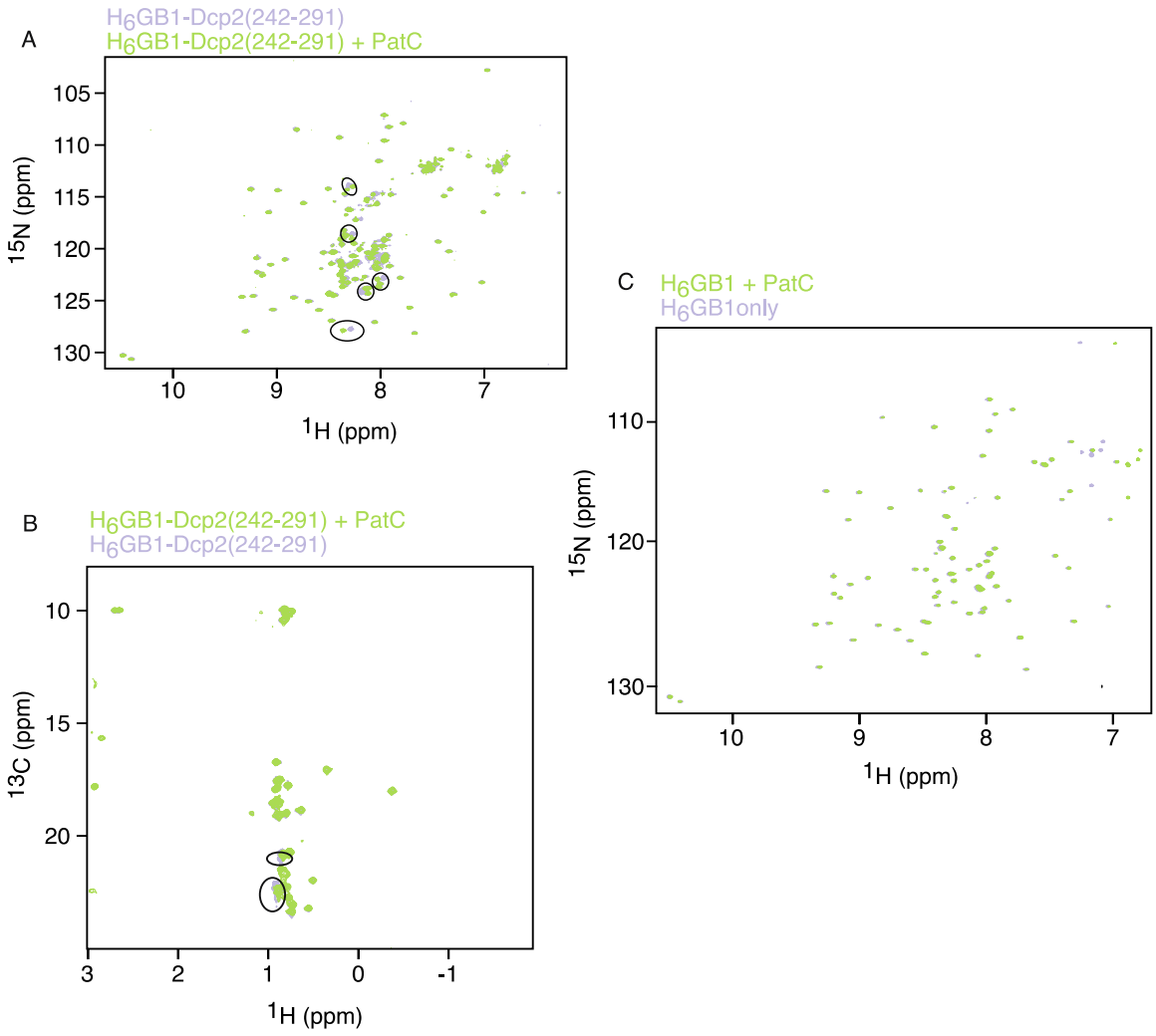

Supplemental Figure 1.5: PatC interacts with an isolated HLM.
A, ^{15}N-^{1}H HSQC of 200µM uniformly ^{15}N labelled H6-GB1-Dcp2 242-291 (purple) alone or 100µM H6-GB1-Dcp2 242-291 with 200µM PatC (green). Circles indicate sites of chemical shift perturbations. **B,** ^{13}C-^{1}H HSQC of 200µM ^{13}C ILV labeled H6-GB1-Dcp2 242-291alone (purple) or 100µM H6-GB1-Dcp2 242-291 with 200µM PatC (green). **C,** No chemical shifts of 50µM ^{15}N-^{1}H HSQC H6-GB1 in the presence of 100µM PatC (purple). 100µM H6-GB1 alone is shown in green.

Supplemental Tables

Supplemental Table 1.1: S.pombe strains used in this study.

Identifier	Strain	Reference
WT	h+ ade6-M210 ura4-D18 leu1-32	Bioneer
ΔPat1	h+ *pat1::kanMX*	Bioneer
spJL-001 (FL-Pat1)	h+ Δ*pat1::pat1:sfGFP:ura4t:hygMX*	This Study
spJL-002 (PatMC)	h+ Δ*pat1::pat1(296-754):sfGFP:ura4t:hygMX*	This Study
spJL-003 (PatC)	h+ Δ*pat1::pat1(440-754):sfGFP:ura4t:hygMX*	This Study
spJL-004 (PatM)	h+ Δ*pat1::pat1(296-439):sfGFP:ura4t:hygMX*	This Study
spJL-005 (MBP-PatMC)	h+ *pat1::MBP:pat1(296-754):sfGFP:ura4t:hygMX*	This Study
spJL-006 (MBP-PatΔLAR)	h+ Δ*pat1::MBP:pat1(317-754):sfGFP:ura4t:hygMX*	This Study
spJL-007 (MBP-Pat(343-754))	h+ Δ*pat1::MBP:pat1(343-754):sfGFP:ura4t:hygMX*	This Study

References

Al-sady B, Greenstein RA, El-samad HJ, Braun S, Madhani HD. 2016. Sensitive and Quantitative Three-Color Protein Imaging in Fission Yeast Using Spectrally Diverse , Recoded Fluorescent Proteins with Experimentally-Characterized In Vivo Maturation Kinetics. *PLoS One* **11**.

Badis G, Saveanu C, Fromont-Racine M, Jacquier A. 2004. Targeted mRNA degradation by deadenylation-independent decapping. *Mol Cell* **15**: 5–15.

Bonnerot C, Boeck R, Lapeyre B. 2000. The Two Proteins Pat1p (Mrt1p) and Spb8p Interact In Vivo, Are Required for mRNA Decay, and Are Functionally Linked to Pab1p. *Mol Cell Biol* **20**: 5939–5946.

Bouveret E. 2000. A Sm-like protein complex that participates in mRNA degradation. *EMBO J* **19**: 1661–1671.

Braun JE, Tritschler F, Haas G, Igreja C, Truffault V, Weichenrieder O, Izaurralde E. 2010. The C-terminal α-α superhelix of Pat is required for mRNA decapping in metazoa. *EMBO J* **29**: 2368–2380.

Charenton C, Gaudon-Plesse C, Fourati Z, Taverniti V, Back R, Kolesnikova O, Séraphin B, Graille M. 2017. A unique surface on Pat1 C-terminal domain directly interacts with Dcp2 decapping enzyme and Xrn1 5′–3′ mRNA exonuclease in yeast. *Proc Natl Acad Sci* **114**: E9493–E9501.

Chowdhury A, Kalurupalle S, Tharun S. 2013. Pat1 contributes to the RNA binding activity of the Lsm1-7 – Pat1 complex. *RNA* **20**: 1465–1475.

Chowdhury A, Mukhopadhyay J, Tharun S. 2007. The decapping activator Lsm1p-7p-Pat1p complex has the intrinsic ability to distinguish between oligoadenylated and polyadenylated RNAs. *RNA* **13**: 998–1016.

Dong S, Li C, Zenklusen D, Singer RH, Jacobson A, He F. 2007. YRA1 Autoregulation Requires Nuclear Export and Cytoplasmic Edc3p-Mediated Degradation of Its Pre-mRNA. *Mol Cell* **25**: 559–573.

Dunckley T, Parker R. 1999. The DCP2 protein is required for mRNA decapping in Saccharomyces cerevisiae and contains a functional MutT motif. *EMBO J* **18**: 5411–5422.

Eswar N, Webb B, Marti-Renom MA, Madhusudhan MS, Eramian D, Shen M, Pieper U, Sali A. 2006. *Comparative protein structure modeling using Modeller*.

Forsburg SL, Rhind N. 2006. Basic Methods for Fission Yeast. *Yeast* **23**: 173–183.

Fourati Z, Kolesnikova O, Back R, Keller J, Charenton C, Taverniti V, Plesse CG, Lazar N, Durand D, Van Tilbeurgh H, et al. 2014. The C-terminal domain from S. cerevisiae Pat1 displays two conserved regions involved in decapping factor recruitment. *PLoS One* **9**.

Franks TM, Lykke-Andersen J. 2008. The Control of mRNA Decapping and P-Body Formation. *Mol Cell* **32**: 605–615.

Fromm SA, Truffault V, Kamenz J, Braun JE, Hoffmann NA, Izaurralde E, Sprangers R. 2012. The structural basis of Edc3-and Scd6-mediated activation of the Dcp1:Dcp2 mRNA decapping complex. *EMBO J* **31**: 279–290.

Guo H, Ingolia NT, Weissman JS, Bartel DP. 2010. Mammalian microRNAs predominantly act to decrease target mRNA levels. *Nature* **466**: 835–840.

Haas G, Braun JE, Igreja C, Tritschler F, Nishihara T, Izaurralde E. 2010. HPat provides a link between deadenylation and decapping in metazoa. *J Cell Biol* **189**: 289–302.

He F, Celik A, Wu C, Jacobson A. 2018. General decapping activators target different subsets of inefficiently translated mRNAs. *Elife* **7**: 1–30.

He F, Jacobson A. 2015. Control of mRNA decapping by positive and negative regulatory

elements in the Dcp2 C-terminal domain. *RNA* 1633–1647.

He W, Parker R. 2001. The yeast cytoplasmic lsm1/pat1p complex protects mRNA 3′ termini from partial degradation. *Genetics* **158**: 1445–1455.

Hubstenberger A, Courel M, Bénard M, Souquere S, Ernoult-Lange M, Chouaib R, Yi Z, Morlot JB, Munier A, Fradet M, et al. 2017. P-Body Purification Reveals the Condensation of Repressed mRNA Regulons. *Mol Cell* **68**: 144–157.e5.

Jonas S, Izaurralde E. 2013. The role of disordered protein regions in the assembly of decapping complexes and RNP granules. *Genes Dev* **27**: 2628–2641.

Jonas S, Izaurralde E. 2015. Towards a molecular understanding of microRNA-mediated gene silencing. *Nat Rev Genet* **16**: 421–433.

Jones BN, Quang-Dang DU, Oku Y, Gross JD. 2008. *A Kinetic Assay to Monitor RNA Decapping Under Single- Turnover Conditions*. 1st ed. Elsevier Inc.

Kervestin S, Jacobson A. 2012. NMD: A multifaceted response to premature translational termination. *Nat Rev Mol Cell Biol* **13**: 700–712.

Lim J, Ha M, Chang H, Kwon SC, Simanshu DK, Patel DJ, Kim VN. 2014. Uridylation by TUT4 and TUT7 marks mRNA for degradation. *Cell* **159**: 1365–1376.

Mitchell SF, Jain S, She M, Parker R. 2012. Global analysis of yeast mRNPs. *Nat Struct Mol Biol* **20**: 127–133.

Moore MJ. 2005. From birth to death: The complex lives of eukaryotic mRNAs. *Science (80-)* **309**: 1514–1518.

Mugridge JS, Tibble RW, Ziemniak M, Jemielity J, Gross JD. Structure of the activated Edc1-Dcp1-Dcp2-Edc3 mRNA decapping complex with substrate analog poised for catalysis. *Nat Commun*.

Nissan T, Rajyaguru P, She M, Song H, Parker R. 2010. Decapping Activators in Saccharomyces cerevisiae Act by Multiple Mechanisms. *Mol Cell* **39**: 773–783.

Paquette DR, Tibble RW, Daifuku TS, Gross JD. 2018. Control of mRNA decapping by autoinhibition. 1–12.

Parker R. 2012. RNA degradation in Saccharomyces cerevisae. *Genetics* **191**: 671–702.

Pilkington GR, Parker R. 2008. Pat1 Contains Distinct Functional Domains That Promote P-Body Assembly and Activation of Decapping. *Mol Cell Biol* **28**: 1298–1312.

Rissland OS, Norbury CJ. 2009. Decapping is preceded by 3' uridylation in a novel pathway of bulk mRNA turnover. **16**.

Sharif H, Conti E. 2013. Architecture of the Lsm1-7-Pat1 Complex: A Conserved Assembly in Eukaryotic mRNA Turnover. *Cell Rep* **5**: 283–291.

Sharif H, Ozgur S, Sharma K, Basquin C, Urlaub H, Conti E. 2013. Structural analysis of the yeast Dhh1-Pat1 complex reveals how Dhh1 engages Pat1, Edc3 and RNA in mutually exclusive interactions. *Nucleic Acids Res* **41**: 8377–8390.

Stevens a. 1980. Purification and characterization of a Saccharomyces cerevisiae exoribonuclease which yields 5'-mononucleotides by a 5' leads to 3' mode of hydrolysis. *J Biol Chem* **255**: 3080–5.

Teixeira D, Parker R. 2007. Analysis of P-Body Assembly in Saccharomyces Cerevisiae. *Mol Biol Cell* **18**: 2274–2287.

Tharun S, He W, Mayes AE, Lennertz P, Beggs JD, Parker R. 2000. Yeast Sm-like proteins function in mRNA decapping and decay. *Nature* **404**: 515–518.

Tharun S, Muhlrad D, Chowdhury A, Parker R. 2005. Mutations in the Saccharomyces cerevisiae LSM1 gene that affect mRNA decapping and 3′ end protection. *Genetics* **170**:

33–46.

Tharun S, Parker R. 2001. Targeting an mRNA for decapping: Displacement of translation factors and association of the Lsm1p-7p complex on deadenylated yeast mRNAs. *Mol Cell* **8**: 1075–1083.

Van Dijk E, Cougot N, Meyer S, Babajko S, Wahle E, Séraphin B. 2002. Human Dcp2: A catalytically active mRNA decapping enzyme located in specific cytoplasmic structures. *EMBO J* **21**: 6915–6924.

Vindry C, Marnef A, Broomhead H, Twyffels L, Ozgur S, Stoecklin G, Llorian M, Smith CW, Mata J, Weil D, et al. 2017. Dual RNA Processing Roles of Pat1b via Cytoplasmic Lsm1-7 and Nuclear Lsm2-8 Complexes. *Cell Rep* **20**: 1187–1200.

Wang C-Y, Wang Y-T, Hsiao W-Y, Wang S-W. 2017. Involvement of fission yeast Pdc2 in RNA degradation and P-body function. *RNA* **23**: 493–503.

Wang Z, Jiao X, Carr-Schmid A, Kiledjian M. 2002. The hDcp2 protein is a mammalian mRNA decapping enzyme. *Proc Natl Acad Sci* **99**: 12663–12668.

Wu D, Muhlrad D, Bowler MW, Jiang S, Liu Z, Parker R, Song H. 2014. Lsm2 and Lsm3 bridge the interaction of the Lsm1-7 complex with Pat1 for decapping activation. *Cell Res* **24**: 233–246.

Wurm JP, Overbeck J, Sprangers R. 2016. The S. pombe mRNA decapping complex recruits cofactors and an Edc1-like activator through a single dynamic surface. *RNA* **22**: 1360–1372.

Youn J-Y, Dunham WH, Hong SJ, Knight JDR, Bashkurov M, Chen GI, Bagci H, Rathod B, MacLeod G, Eng SWM, et al. 2018. High-Density Proximity Mapping Reveals the Subcellular Organization of mRNA-Associated Granules and Bodies. *Mol Cell* 1–16.

Chapter 2

Pat1 increases the range of decay factors and RNA bound by the Lsm1-7 complex

Joseph H. Lobel[1,2] and John D. Gross[2,*]

[1]Chemistry and Chemical Biology Graduate Program, University of California, San Francisco, San Francisco, California

[2]Department of Pharmaceutical Chemistry, University of California, San Francisco, San Francisco, California

Abstract

Pat1 promotes the activation and assembly of multiple proteins during mRNA decay. After deadenylation, the Pat1/Lsm1-7 complex binds to transcripts containing oligo(A) tails, which can be modified by the addition of several terminal uridine residues. Pat1 enhances Lsm1-7 binding to the 3' end, but it is unknown how this interaction is influenced by nucleotide composition. Here we examine Pat1/Lsm1-7 binding to a series of oligoribonucleotides containing different A/U contents using recombinant purified proteins from fission yeast. We observe a positive correlation between fractional uridine content and Lsm1-7 binding affinity. Addition of Pat1 broadens RNA specificity of Lsm1-7 by enhancing binding to A-rich RNAs and increases cooperativity on all oligonucleotides tested. Consistent with increased cooperativity, Pat1 promotes multimerization of the Lsm1-7 complex, which is potentiated by RNA binding. Furthermore, the inherent ability of Pat1 to multimerize drives liquid-liquid phase separation with multivalent decapping enzyme complexes of Dcp1/Dcp2. Our results uncover how Pat1 regulates RNA binding and higher order assembly by mRNA decay factors.

Introduction

A dense network of protein-protein interactions regulates 5'-3' mRNA decay, which is important for gene expression and many physiological processes including development, microRNA-mediated decay, and quality control mechanisms (Moore 2005; Guo et al. 2010; Conti and Izaurralde 2005). Bulk 5'-3' mRNA degradation begins with the trimming of the 3' poly(A) tail by cytoplasmic deadenylases, which can be followed by addition of several uridines by terminal uridine transferases in fission yeast and metazoans (Parker 2012; Rissland and Norbury 2009; Lim et al. 2014). After deadenylation and subsequent uridylation, the heterooctameric Pat1/Lsm1-7

complex assembles on or near the 3' A/U-rich deadenylated tail of the mRNA (He et al. 2018; Mitchell et al. 2012; Tharun and Parker 2001). Pat1 subsequently activates decapping by Dcp1/Dcp2, leading to rapid 5'-3' degradation of the mRNA body by the conserved exonuclease Xrn1 (Lobel et al. 2019; Wu et al. 2014; Nissan et al. 2010; Stevens 1980; Parker 2012). Pat1 activates proteins at both the 5' and 3' end of the mRNA by enhancing RNA binding of the Lsm1-7 complex to the deadenylated 3' end and decapping by the Dcp1/Dcp2 complex (Lobel et al. 2019; Nissan et al. 2010; Chowdhury et al. 2013; Charenton et al. 2017). Deletion of Pat1 results in accumulation of poorly translated, deadenylated, capped transcripts, suggesting a block in decapping (Wang et al. 2017; He et al. 2018).

Many mRNA decay factors, including Pat1, are enriched in Processing-bodies (P-bodies) which are a class of membraneless organelles that may function in mRNA storage or decay (Teixeira and Parker 2007; Xing et al. 2018; Hubstenberger et al. 2017). At the molecular level, these structures are promoted by multivalent protein-protein and protein-nucleic acid interactions that are required for phase separation. Overexpression of Pat1 enhances P-body formation in fungi, suggesting its importance in assembling these structures (Wang et al. 2017; Sachdev et al. 2019). Therefore, Pat1 functions at multiple steps during 5'-3' mRNA decay to coordinate degradation of the transcript.

Pat1 has three regions and uses a combination of disordered and globular domains to interact with and activate multiple mRNA decay factors. The disordered N-terminus contains a conserved FDF motif that interacts with Dhh1 (DDX6 in humans) and potentiates P-body formation, but is largely dispensable for function (Sachdev et al. 2019; Sharif et al. 2013; Pilkington and Parker 2008). The unstructured middle domain contains multiple short linear interaction motifs (SLiMs) and

cooperates with the structured C-terminal domain to activate RNA binding by Lsm1-7 and decapping by the Dcp1/Dcp2 complex through multiple mechanisms (Lobel et al. 2019; Pilkington and Parker 2008; Chowdhury et al. 2013).

While it is known how Pat1 activates different mRNA decay factors, much less is understood about how it affects specific RNA recognition by Lsm1-7. *In vitro*, budding yeast Pat1/Lsm1-7 shows a preference for oligoadenyated RNAs compared to those containing poly(A) tails; however, genome-wide CLIP studies indicate Pat1/Lsm1 co-occupy the 3' untranslated region (UTR) of budding yeast transcripts without enriching a specific sequence motif (Chowdhury et al. 2007; Mitchell et al. 2012). In fission yeast and metazoan cells, deletion of Lsm1 or Pat1 stabilizes mRNA decay intermediates with oligo(A) tails containing several uridines (Lim et al. 2014; Rissland and Norbury 2009). Furthermore, in mammalian cells, knockdown of Pat1 stabilizes transcripts with AU-rich sequences in the 3' UTR (Vindry et al. 2017). Lsm1-7 can also bind oligo(U) RNA sequence *in vitro* and promotes decay of histone mRNAs that containing U-rich tails in cells (Mullen and Marzluff 2008). How Pat1 affects location and sequence specificity of the Lsm1-7 complex on mRNA is poorly understood.

In this work, we evaluate recombinant purified *S.pombe* Pat1/Lsm1-7 complex binding to a series of oligonucleotides of different A/U content. Lsm1-7 alone has a binding preference for U-rich RNAs. Addition of Pat1, however, broadens the specificity of the Lsm1-7 complex by enhancing binding to A-rich targets. Furthermore, Pat1 increases cooperative binding of Lsm1-7 to oligonucleotides, which drives multimerization of the heterooctamer on RNA in a sequence independent manner. Oligomerization is an inherent property of Pat1 permits higher order

assembly with multivalent Dcp1/Dcp2 complexes, which can recruit additional mRNA decay machinery. Taken together, this work reveals how Pat1 broadens the specificity of Lsm1-7 and promotes the assembly size of higher order decapping complexes.

Results

The PatMC/Lsm1-7 complex cooperatively binds to A-rich RNA

Previous studies indicate that the middle and C-terminal domains of Pat1 (termed PatMC) are sufficient to support cell growth in yeast (Pilkington and Parker 2008; Lobel et al. 2019). To understand how different 3' end sequences influence PatMC/Lsm1-7 binding, we tested recombinant purified *S.pombe* Lsm1-7 complexes alone or coexpressed with PatMC for their ability to bind different oligo-RNAs by fluorescence polarization (**Fig. 2.1A-B)**. Because global profiling of RNA tails indicate that uridine residues are found on short tails (<25 nt), we investigated a series of 15mers containing different adenine and uracil contents (Chang et al. 2014; Rissland and Norbury 2009). As seen previously, PatMC enhanced the RNA binding of Lsm1-7 to A15 RNA by an order of magnitude (Lobel et al. 2019). The fold-enhancement of Lsm1-7 RNA binding by PatMC strongly correlated with the fractional adenine content of the 15mer, where a greater difference in free energy of binding was observed for more adenine-rich substrates **(Fig. 2.1C & S2.1A-F)**. Furthermore, the Lsm1-7 complex alone strongly favored binding to U-rich 15mers, which was not affected by PatMC. This suggests that PatMC may serve to selectively enhance RNA binding of Lsm1-7 to adenine rich tails and may be dispensable for engaging U-rich tails.

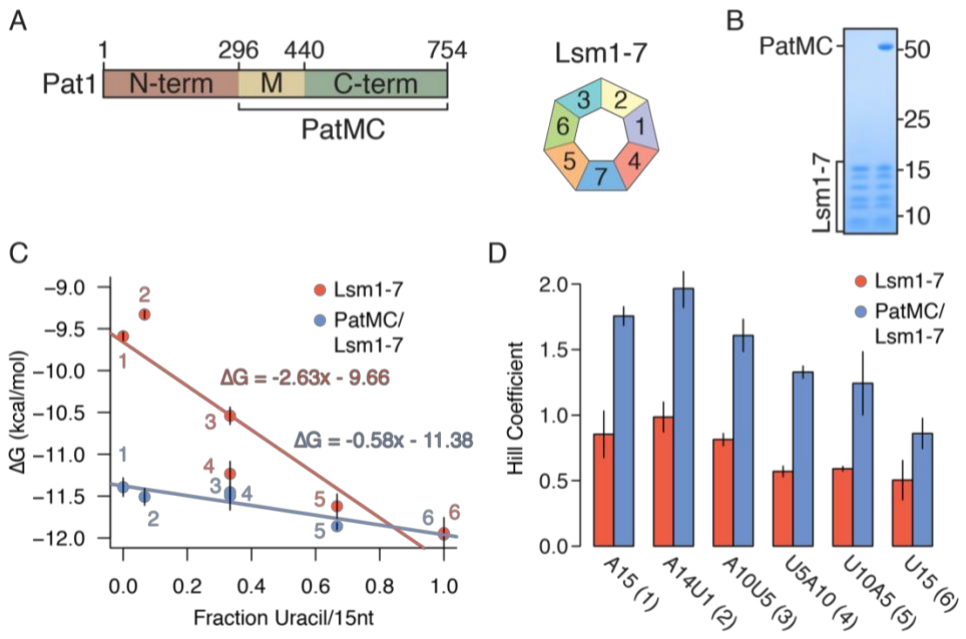

Figure 2.1: PatMC enhances Lsm1-7 binding to Adenine-rich substrates in a cooperative manner
A, Schematic of Pat1 domains and Lsm1-7 **B,** SDS-PAGE of the Lsm1-7 complex alone (left) or with PatMC (right). Molecular weight (kDa) shown on right. **C,** Lsm1-7 or PatMC/Lsm1-7 binding to different 5'-FAM labelled 15mer RNAs (A15, A14U1, A10U5, U5A10, U10A5, U15) monitored by fluorescence polarization. Numbers correspond to labels in **D**. Binding affinities were converted to ΔG and plotted against the fractional uracil content of the oligonucleotides (n=3). **D,** Hill coefficients for each fit for the binding isotherms shown in **C** (n=3).

In addition to the differences in affinities for the oligonucleotides, we also observed a difference in Hill coefficients, a measure of cooperativity that places a lower bound on the number of Pat1/Lsm1-7 complexes binding RNA. The binding isotherms of the PatMC/Lsm1-7 complex were consistently ~2 fold more cooperative than Lsm1-7 alone for all tested RNAs, suggesting that PatMC/Lsm1-7 may be engaging A15 and U15 RNA in a different manner **(Fig. 2.1D)**. Specifically, PatMC/Lsm1-7 had a Hill coefficient of ~1 for U15 RNA and ~2 for A15 RNA. This indicates that at least one or two copies of the PatMC/Lsm1-7 complex cooperatively bind to U15 or A15 RNA, respectively.

Short RNAs are sufficient to promote dimerization of the PatMC/Lsm1-7 complex

To directly test the number of PatMC/Lsm1-7 complexes bound to short oligonucleotides, we used size exclusion chromatography coupled to multiangle light scattering (SEC-MALS). The SEC step fractionates protein complexes by hydrodynamic radius and molar mass is concurrently detected by light-scattering and differential refractometry (Wyatt 1993). The PatMC/Lsm1-7 complex was incubated with stoichiometric amounts of A15 RNA and subjected to SEC-MALS. The A15 RNA promoted the formation of two peaks that had identical protein composition and molar masses corresponding to that of a dimeric (two copies of PatMC/Lsm1-7) and tetrameric assembly **(Fig. 2.2A, Table 1)**. Shorter RNAs, such as A10, also promoted oligomeric PatMC/Lsm1-7 assemblies, with molar masses corresponding to dimeric and tetrameric complexes **(Fig. 2.2B)**. However, we observed that the A10 RNA reduced tetramerization and instead produced predominantly dimeric PatMC/Lsm1-7 complexes, based on the relative ratio of the peaks in the chromatogram. This suggests that RNA length many influence tetramerization, but short RNAS still promote higher order assembly of the PatMC/Lsm1-7 complex.

To evaluate the stability of the oligomeric assemblies, we performed sedimentation velocity analytical ultracentrifugation (SV-AUC) on PatMC/Lsm1-7 with stoichiometric amounts of A15 RNA over the course of 12 hours. While we could detect a strong dimeric peak in the sedimentation distribution, there was minimal amounts of tetrameric assemblies **(Fig. 2.2C)**. Furthermore, the tetrameric fraction of the PatMC/Lsm1-7/A15 complex disassembled into dimers and tetramers upon reinjection over a size exclusion column, while the dimeric peak did not further dissociate (**Fig. S2.2A-C)**. This suggests that the tetrameric PatMC/Lsm1-7/RNA complex results from weak interactions between two PatMC/Lsm1-7/RNA dimers.

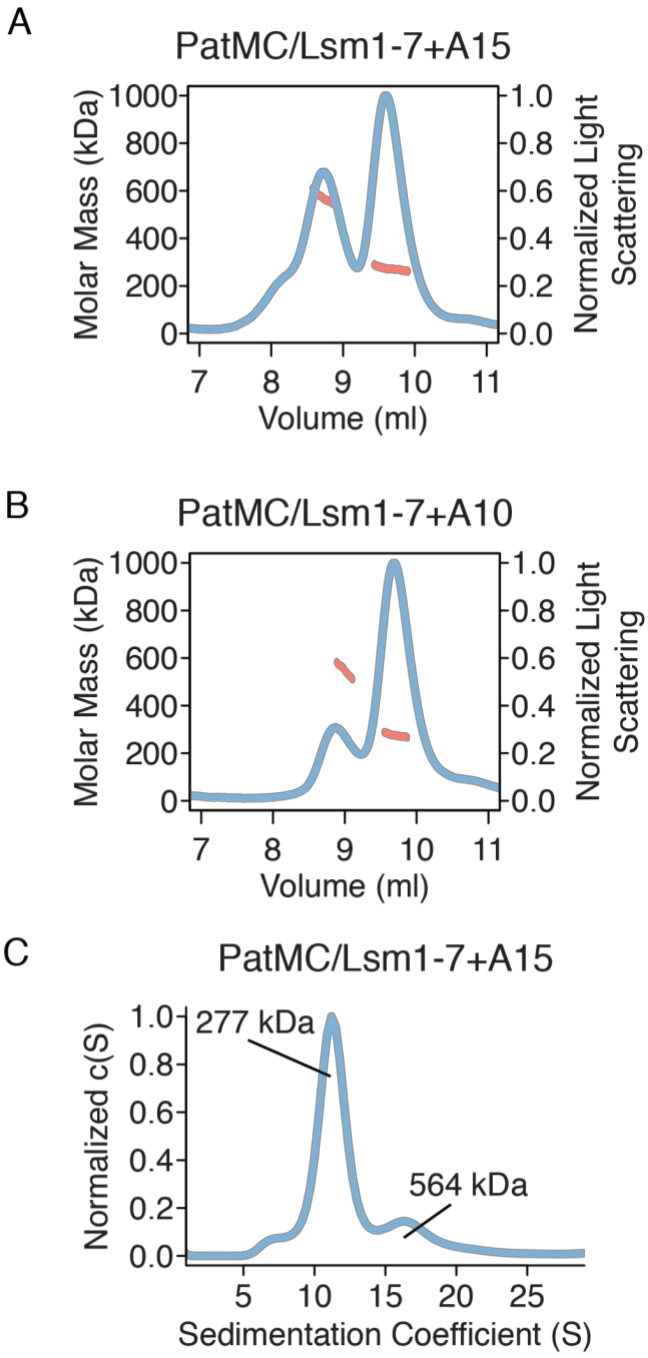

Figure 2.2: RNA promotes stable dimerization of the PatMC/Lsm1-7 complex
A-B, SEC-MALS of 20.6 µM PatMC/Lsm1-7 with **A,** A15 and **B, A10**. Expected and observed molar masses are shown in Table 1. **C,** SV-AUC of 9.3 µM PatMC/Lsm1-7 with stoichiometric amounts of A15 RNA at 250 mM NaCl. c(S) is the sedimentation distribution with molecular weights determined from fits.

We next asked how PatMC/Lsm1-7 assembled on U15 RNA. As seen with A15 RNA, addition of stoichiometric amounts of U15 to the PatMC/Lsm1-7 complex resulted in two peaks by SEC-MALS with molar masses corresponding to dimeric and tetrameric assemblies **(Fig. 2.3A/B)**. This effect depends on PatMC, because Lsm1-7 alone bound to U15 RNA remained monomeric (**Fig. 2.3C**). Taken together, this indicates that PatMC promotes the higher order assembly of the PatMC/Lsm1-7 complex on both A15 and U15 RNA.

It is possible that that each PatMC/Lsm1-7 complex binds an individual RNA or that multiple PatMC/Lsm1-7 complexes co-occupy a single RNA to promote oligomerization. To test these possibilities, we determined the stoichiometry of PatMC/Lsm1-7 binding to RNA. Experiments were performed under saturating conditions, where concentration of the oligo-RNA was far above the K_d. Binding of labelled U15 was followed by fluorescence anisotropy. Titration of Lsm1-7 alone or the PatMC/Lsm1-7 complex results in saturation of the anisotropy signal at one equivalent of RNA, indicating 1:1 binding between PatMC/Lsm1-7 and the U15 oligonucleotide. Similar results were obtained for PatMC/Lsm1-7 binding to A15 (**Fig. S2.3**). This indicates that each PatMC/Lsm1-7 heterooctamer binds a single oligo-RNA, though we cannot exclude the possibility that PatMC/Lsm1-7 can co-occupy RNA sequences longer than 15nt tested here. Therefore, we conclude that RNA ligands of different sequences and lengths induce stable dimerization of the PatMC/Lsm1-7 complex.

Multimerization is an intrinsic property of the PatMC/Lsm1-7 complex

As PatMC/Lsm1-7 binds to RNA as a higher order assembly, we asked if the complex had the intrinsic ability to multimerize in the absence of RNA. While PatMC/Lsm1-7 initially purified as

a monomer, concentration and subsequent SEC-MALS of the complex in the absence of RNA revealed two peaks with molar masses corresponding to monomeric and dimeric PatMC/Lsm1-7 complexes **(Fig. 2.4A-C)**. This indicates that the PatMC/Lsm1-7 complex has the inherent ability to form multimers independent of nucleic acid, and suggests that RNA may drive higher order assembly.

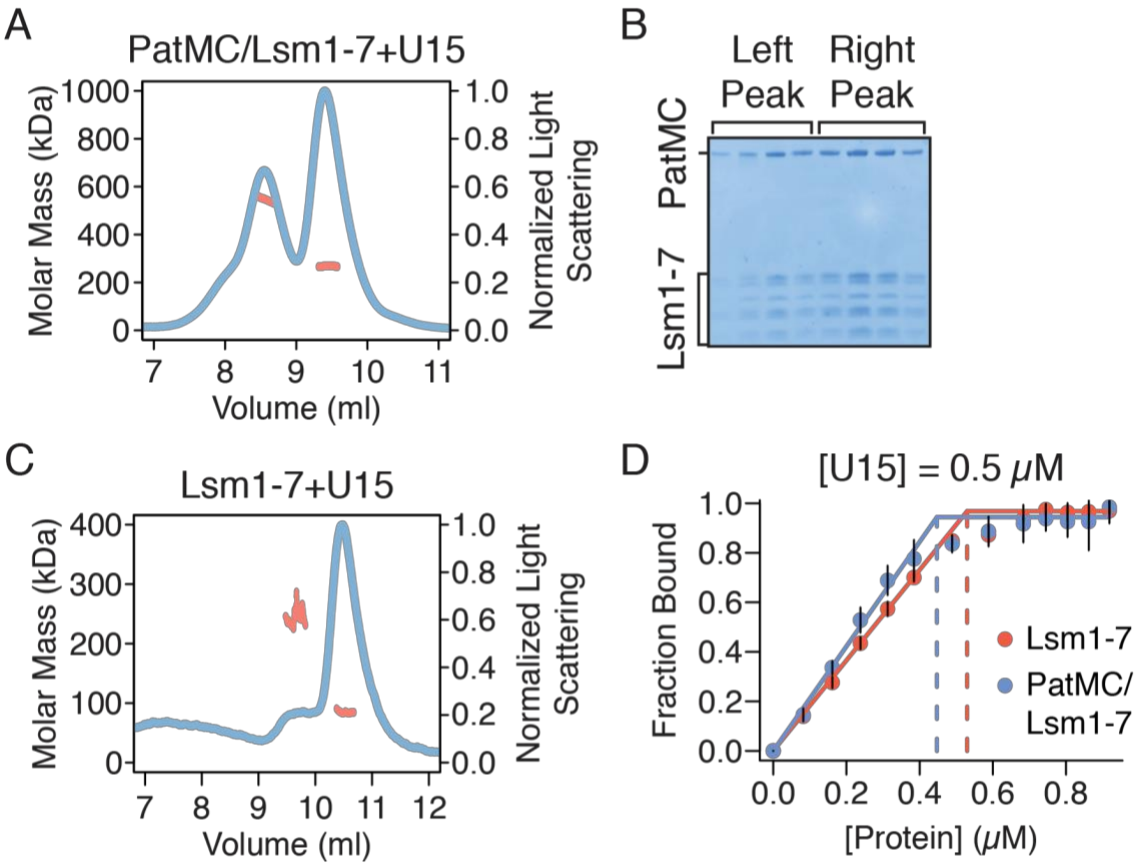

Figure 2.3: Multiple RNA sequences drive higher order PatMC/Lsm1-7 assembly in a Pat1 dependent manner

A, SEC-MALS of 20.6 µM PatMC/Lsm1-7 with U15 RNA. The expected molar mass of the monomeric PatMC/Lsm1-7 complex is 133 kDa. **B,** Representative SDS-PAGE gel of fractions in **A. C,** SEC-MALS of 20.6 µM Lsm1-7 with U15 RNA. The expect mass of the monomeric Lsm1-7 complex is 81 kDa. Expected and observed molar masses are shown in Table 1. **D,** Stoichiometry analysis of Lsm1-7 or PatMC/Lsm1-7 with 5'-FAM labelled U15 RNA at 0.5 µM, which is >100-fold above k_d.

To test the stability of the assemblies in the absence of RNA, we performed SV-AUC on the PatMC/Lsm1-7 complex alone. Over the course of 12 hours, we observed both a monomeric and dimeric species, indicating that both these complexes were stable **(Fig. 2.4D)**. Furthermore, increasing salt concentrations favored monomerization of the complex, indicating PatMC/Lsm1-7 oligomerization is reversible **(Fig. S2.4)**. Because Lsm1-7 was monomeric in the absence of PatMC, the above results indicate PatMC drives multimerization of Lsm1-7, which may be enhanced by RNA binding (**Fig. 2.2A & 2.3A)**.

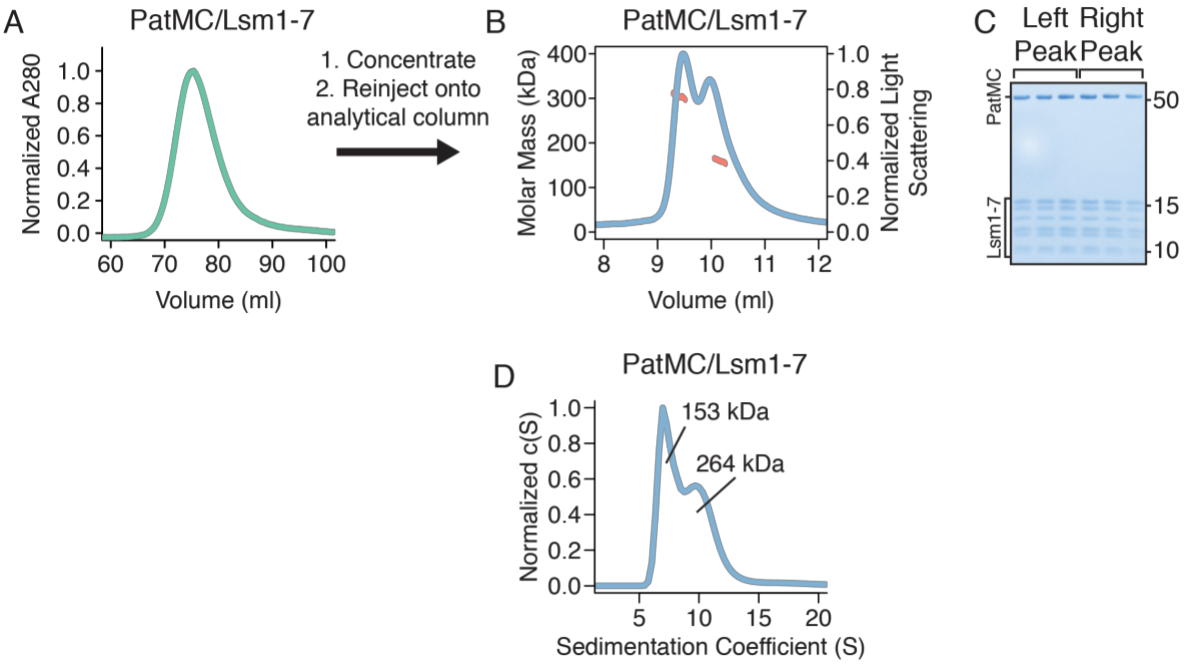

Figure 2.4: The PatMC/Lsm1-7 complex can intrinsically form a dimeric complex
A, Preparative size exclusion chromatography of the PatMC/Lsm1-7 complex in a 400 mM NaCl buffer. **B,** SEC-MALS of the concentrated PatMC/Lsm1-7 complex at 250 mM NaCl. The expected mass of the monomeric PatMC/Lsm1-7 complex is 133 kDa. Expected and observed molar masses are shown in Table 1. **C,** Representative SDS-PAGE gel of peaks (Left to right: earlier to later elution volumes). **D,** SV-AUC of 9.3 µM PatMC/Lsm1-7 at 250 mM NaCl. c(S) is the sedimentation distribution with molecular weights determined from fits.

PatMC promotes liquid-droplet formation with Dcp2 and recruits additional mRNA decay factors

Previous studies demonstrate that the monomeric, globular C-terminal domain of Pat1 can bind helical leucine motifs (HLMs) in the disordered C-terminus of Dcp2 (Charenton et al. 2017; Lobel et al. 2019). Known dimeric HLM binding proteins, such as Edc3, can interact with Dcp2 and undergo liquid-liquid phase separation with Dcp2 constructs that contain multiple HLMs (Schutz et al. 2017; Fromm et al. 2014). Our biochemical data demonstrate that PatMC can inherently oligomerize in the absence of RNA, so we tested if it could promote liquid-liquid phase separation with multivalent Dcp1/Dcp2 complexes, analogous to Edc3. PatMC purified was purified fused to maltose-binding protein (MBP) to enhance its solubility (see Methods). It was then mixed with an extended Dcp2 construct containing both the catalytic core and three HLMs with its obligate cofactor Dcp1 (Dcp1/Dcp2 1-504, termed Dcp1/Dcp2$_{Ext}$) **(Fig. 2.5A)**. Though neither PatMC nor Dcp1/Dcp2$_{Ext}$ formed condensates individually, mixing stoichiometric amounts of Dcp1/Dcp2$_{Ext}$ with MBP-PatMC resulted in formation of phase separated droplets (**Fig 2.5B and not shown)**.

To understand the requirements of PatMC and Dcp1/Dcp2$_{Ext}$ for droplet formation, we queried how individual regions of both complexes contribute to phase separation. The C-terminal domain of Pat1 is monomeric and binds HLMs, but did not promote phase separation of Dcp1/Dcp2$_{Ext}$ (**Fig. 2.5B**). Additionally, PatMC did not phase separate with a Dcp1/Dcp2 complex containing a single HLM (Dcp2 residues 1-266, termed Dcp2$_{HLM1}$) **(Fig. 2.5B)**. These data suggest that the middle and C-terminal domains of Pat1 promote phase separation of Dcp1/Dcp2 by driving self-association and binding HLMs on Dcp2, respectively. We conclude PatMC oligomerization promotes phase separation with multivalent cofactors such as Dcp2.

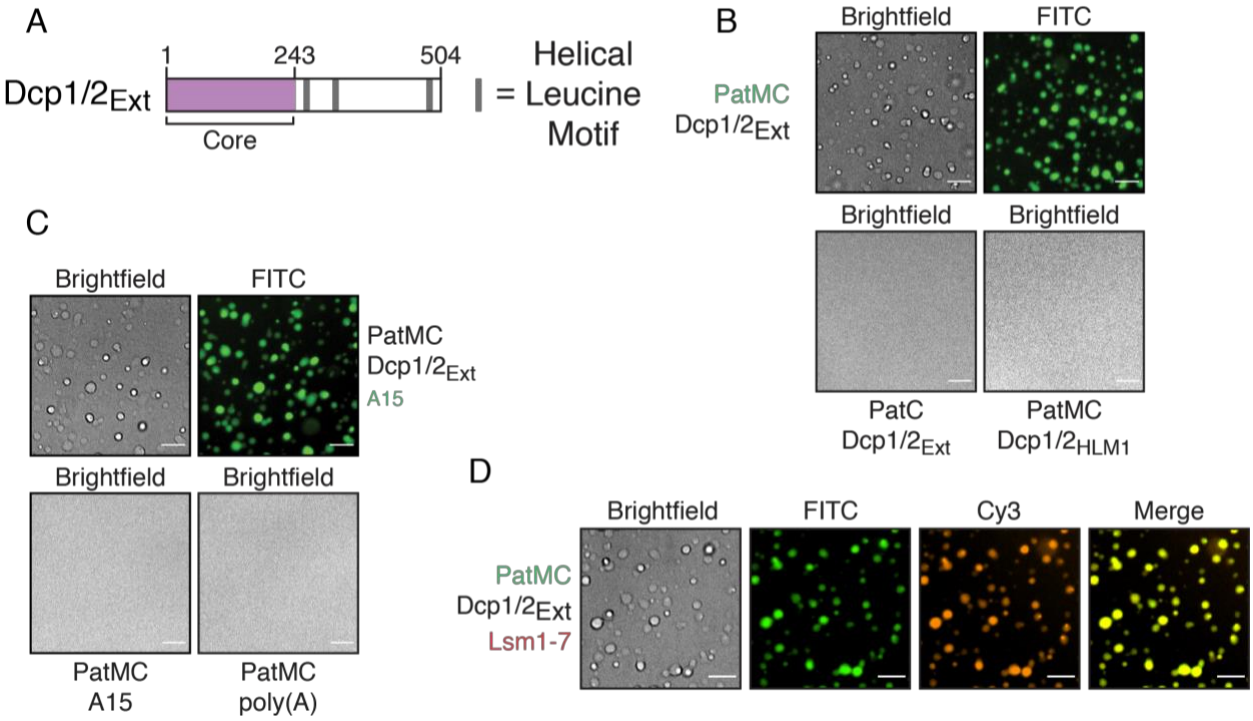

Figure 2.5: Oligomerization of PatMC promotes liquid-liquid phase separation with Dcp2 and recruitment of additional RNA decay machinery
A, Schematic of Dcp2 construct used. Purple represents the globular domain that cleaves the m7G cap. Gray bars represent helical leucine motifs in the disordered C-terminal extension. **B,** Brightfield and fluorescence microscopy of droplets with 2.5 µM Pat constructs (0.1 µM FITC-labeled) with stoichiometric amounts of Dcp1/Dcp2Ext. **C,** Brightfield and fluorescence microscopy of droplets with 2.5 µM PatMC and 2.5 µM rA15 RNA or 13.4 ng/µl poly(A) RNA with or without 2.5 µM Dcp1/Dcp2Ext and 0.1 µM FAM-rA15. **D,** Brightfield and fluorescence microscopy of 2.5 µM PatMC (0.1 µM FITC-labelled) and Dcp1/Dcp2Ext with 0.1 µM Alexa555 labelled Lsm1-7. All images taken at 40x magnification. Scale bar, 10 µm.

PatMC and Dcp2 both interact with RNA, which can trigger or potentiate liquid-liquid phase separation with oligomeric RNA binding proteins (RBPs) (Mugler et al. 2016; Lin et al. 2015). The PatMC/Dcp1/Dcp2Ext droplets were able to incorporate A15 RNA, though A15 RNA did not change the critical concentration required for phase separation (**Fig. 2.5C & S2.5A)**. However, neither short A15 RNAs nor poly(A) RNA promoted droplet formation with either PatMC or Dcp1/Dcp2Ext alone (**Fig. 2.5C and data not shown**). RNA could not trigger phase separation

with either Dcp1/Dcp2$_{Ext}$ or PatMC alone, suggesting that the protein-protein interactions are the primary driver of phase separation between PatMC and Dcp2.

We next asked if other mRNA decay factors could be incorporated in PatMC/Lsm1-7 droplets. Lsm1-7, but not a nonspecific protein, was recruited of pre-formed PatMC/Dcp1/Dcp2$_{Ext}$ condensates, indicating that PatMC can bridge both 5' (Dcp1/Dcp2) and 3' (Lsm1-7) decay factors in the context of the phase separated droplet (**Fig. 2.5D & S2.4C**). Lsm1-7 neither phase separates with PatMC nor affected the critical concentration for droplet formation, consistent with Lsm1-7 being a monomeric complex (**Fig. S2.5A & S2.5B**). Furthermore, Dcp1/Dcp2$_{Ext}$/PatMC/Lsm1-7 condensates recruited RNA (**Fig. S2.5D**). These observations suggest that Pat1 may bridge both 5' and 3' activities in the context of a phase separated droplet.

Discussion

Our biochemical reconstitution uncovers how Pat1 broadens the specificity of the Lsm1-7 complex and promotes higher order assembly of multiple mRNA decay factors. First, Pat1 expands the Lsm1-7 complex's sequence preference by enhancing binding to adenine-rich RNAs. Second, PatMC promotes cooperative binding of Lsm1-7 to RNA, which drives oligomerization on nucleic acid. Third, the PatMC/Lsm1-7 complex has the inherent ability to oligomerize, which is dependent on Pat1 and consistent with coimmunoprecipitation data fission yeast. Finally, we show that an oligomeric PatMC drives phase separation with multivalent Dcp1/Dcp2 complexes that can recruit RNA and additional decay factors to droplets. Taken together, this biochemically reconstituted system reveals how Pat1 increases the range of RNA targets bound by the Lsm1-7 complex and facilitates higher order assembly of multiple decapping factors (**Fig. 2.6A/B)**.

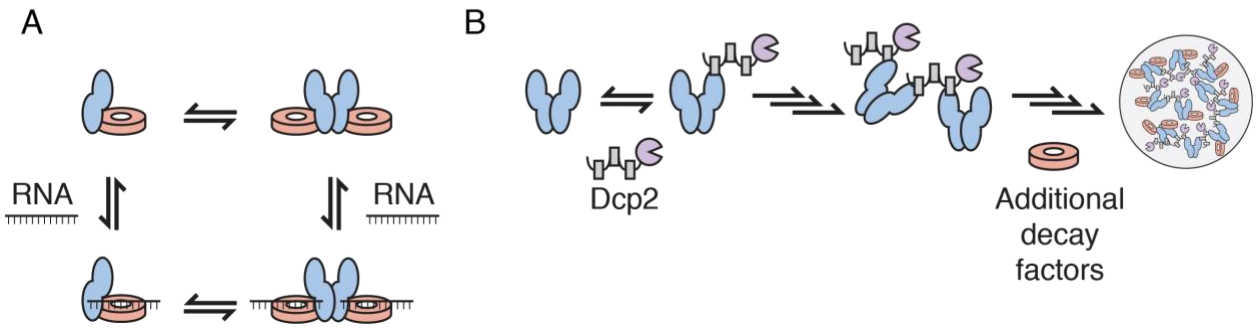

Figure 2.6: Model for how Pat1 increases specificity and assembly for different mRNA decay factors
A, Potential thermodynamic coupling between Pat1 (blue), Lsm1-7 (red), and RNA binding to promote multimerization of the Pat1/Lsm1-7 complex. **B,** Binding of oligiomeric Pat1 assemblies to multivalent Dcp1/Dcp2 complexes promotes phase separation and recruitment of additional mRNA decay factors.

The Lsm1-7 ring is the high affinity RNA binding component of the Pat1/Lsm1-7 complex and has a preference for U-rich oligonucleotides (Wu et al. 2014; Lobel et al. 2019; Chowdhury et al. 2007). Pat1 broadens the specificity of the Lsm1-7 complex by enhancing the affinity of Lsm1-7 for oligonucleotides with higher adenine content (Lobel et al. 2019; Chowdhury et al. 2013) (**Fig. 2.1**). We speculate that Pat1 may allow the Lsm1-7 complex to bind sequences which it has inherently weaker affinity for and therefore expand the complex's target repertoire.

Though PatMC increases the range of RNA substrates bound by Lsm1-7, it is unclear all RNA targets bind in the same manner. For example, PatMC does not enhance the affinity of Lsm1-7 for U15 RNA, in contrast to A15 RNA or A/U rich RNA. Moreover, higher adenine contents favors more cooperative binding of PatMC/Lsm1-7. On the other hand, Pat1/Lsm1-7 stoichiometrically binds all RNA targets as a stable dimer. Determining the binding modes of different RNAs with the Pat1/Lsm1-7 complex remains a challenge for future structural studies.

PatMC also consistently increased the cooperativity of Lsm1-7 binding to all oligonucleotides tested, suggesting a coupling between protein-protein interactions and RNA binding. In support, addition of RNAs drive formation of stable dimeric PatMC/Lsm1-7 assembly whereas in the absence of RNA, PatMC/Lsm1-7 exists in monomer/dimer equilibrium. This suggests two possible pathways which the PatMC/Lsm1-7 complex can load onto RNA. First, RNA may bind to dimeric PatMC/Lsm1-7 from a pre-existing monomer/dimer equilibrium. Alternatively, RNA could bind monomeric PatMC/Lsm1-7 which then forms a dimer (**Fig. 2.6A**). These pathways, could in fact, be part of a thermodynamic cycle, which is in qualitative agreement with our observations.

The discovery that Pat1 has the ability to oligomerize is reminiscent of the homo-hexameric bacterial Lsm protein, Hfq, and its cofactor Crc. Recent work has demonstrated that two copies of Crc can bridge two Hfq hexamers in an RNA dependent manner (Pei et al. 2019; Sonnleitner et al. 2018). While the details of higher order Lsm assemblies between bacteria and eukaryotes differ, oligomerization may be a conserved feature of Lsm complexes and their cofactors.

The inherent ability of PatMC to oligomerize drives phase separation with multivalent cofactors, such as Dcp2 containing multiple HLMs. This derives from multivalent interactions between Dcp2 and oligomeric PatMC. These droplets can recruit Lsm1-7, providing evidence that Pat1 can bring both 5' and 3' mRNA decay factors in close proximity in the context of these phase separated droplets (**Fig. 5**). Additional partners of Pat1, such as Dhh1, may cooperate to further promote droplet formation (Sachdev et al. 2019). Nucleating high local concentration of multiple decapping RBPs in the context of a phase separated droplet may be leveraged for 5' and 3' end

communication during decay (**Fig. 2.6B**). Future work is required to understand how an oligomeric Pat1 is regulated and functions in assembling an active decapping mRNP during 5'-3' mRNA decay.

Tables

Table 2.1: Expected and observed molar masses from SEC-MALS
Expected and observed molar masses of SEC-MALS chromatograms. Error is displayed in parenthesis to the right of observed peak. Peak 1 and 2 refers to the earlier and later elution volume peaks, respectively.

Protein + RNA Complex	Expected Monomer Molar Mass (kDa)	Observed Molar Mass, Peak 1 (kDa)	Observed Molar Mass, Peak 2 (kDa)
PatMC/Lsm1-7	133.5	304.5 (± 1.20%)	160.3 (± 0.93%)
PatMC/Lsm1-7 + A15	138.2	576.0 (± 1.28%)	273.3 (± 0.56%)
PatMC/Lsm1-7 + A10	136.6	554.2 (± 0.80%)	275.5 (± 0.26%)
PatMC/Lsm1-7 + U15	137.8	548.1 (± 0.91%)	268.1 (± 0.88%)
Lsm1-7 + U15	85.6	86.1 (± 2.40%)	N/A

Supplemental Figures

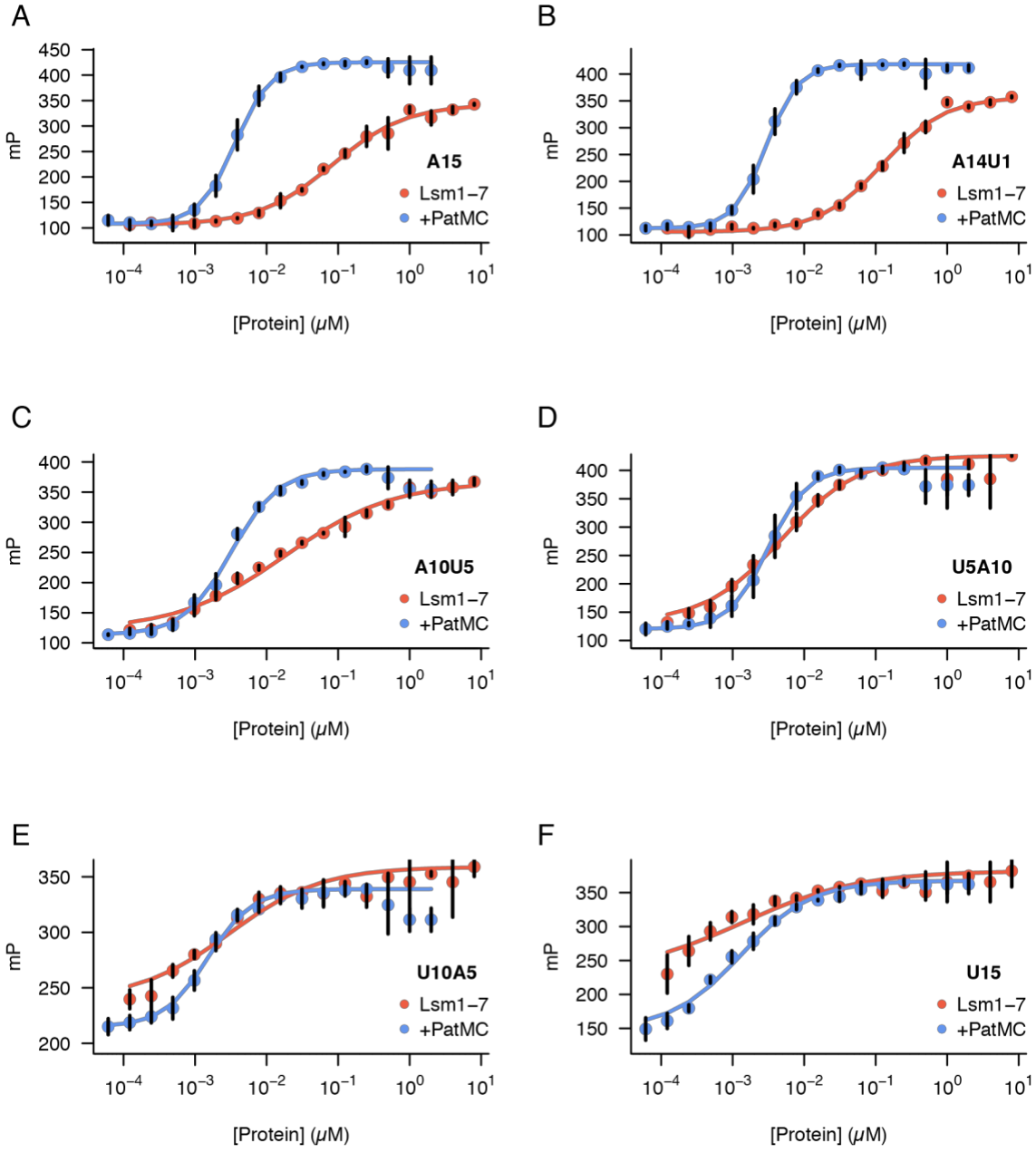

Supplemental Figure 2.1: Binding of Lsm1-7 +/- PatMC to different RNAs
A-F, Lsm1-7 or PatMC/Lsm1-7 binding to **A,** A15 **B,** A14U1 **C,** A10U5 **D,** U5A10 **E,** A5U10 **F,** U15 (n = 3 for all).

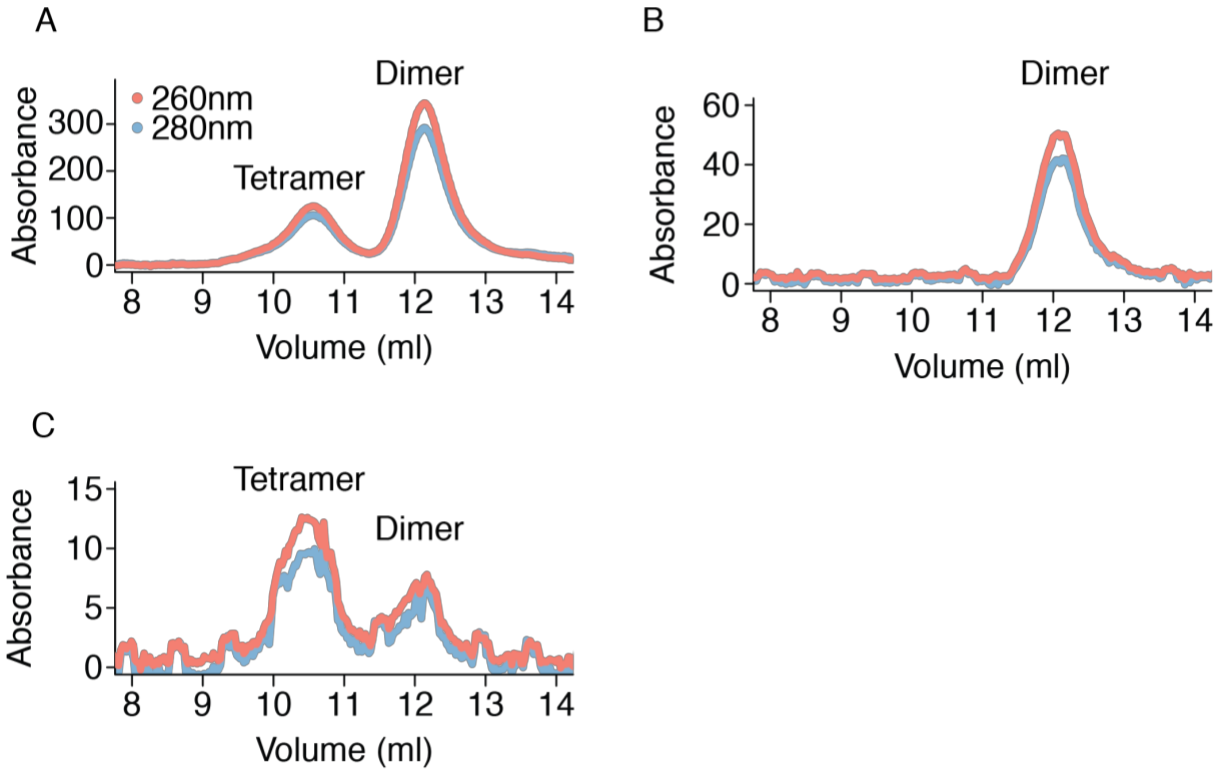

Supplemental Figure 2.2: The dimeric PatMC/Lsm1-7/RNA assembly is stable
A, Analytical size exclusion chromatography of PatMC/Lsm1-7 with A15 RNA. Peaks corresponding to dimer and tetramer are labelled. **B,** Reinjection of peak corresponding to the dimeric PatMC/Lsm1-7 complex. **C,** Reinjection of the peak corresponding to the tetrameric PatMC/Lsm1-7 complex. All conditions were in a 250 mM NaCl buffer. The 260 and 280 nm absorbances are displayed in red and blue, respectively.

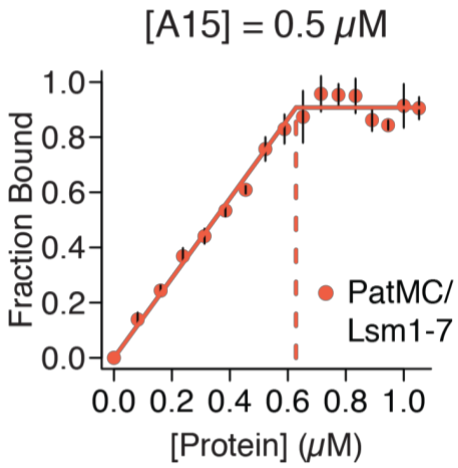

Supplemental Figure 2.3: PatMC/Lsm1-7 binds A15 stoichiometrically
Stoichiometry analysis of Lsm1-7 or PatMC/Lsm1-7 with 5'-FAM labelled A15 RNA at 0.5 µM, which is ~100-fold above k_d.

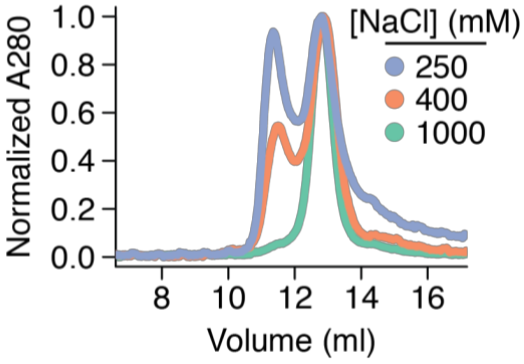

Supplemental Figure 2.4: The monomer/dimer equilibrium of the PatMC/Lsm1-7 complex is sensitive to ionic strength of solution.
Analytical size exclusion chromatography of PatMC/Lsm1-7 complexes in different ionic strength solutions as indicated in the figure legend. All protein was run in 20 mM HEPES pH 7.0, 1 mM DTT and the specified NaCl concentration.

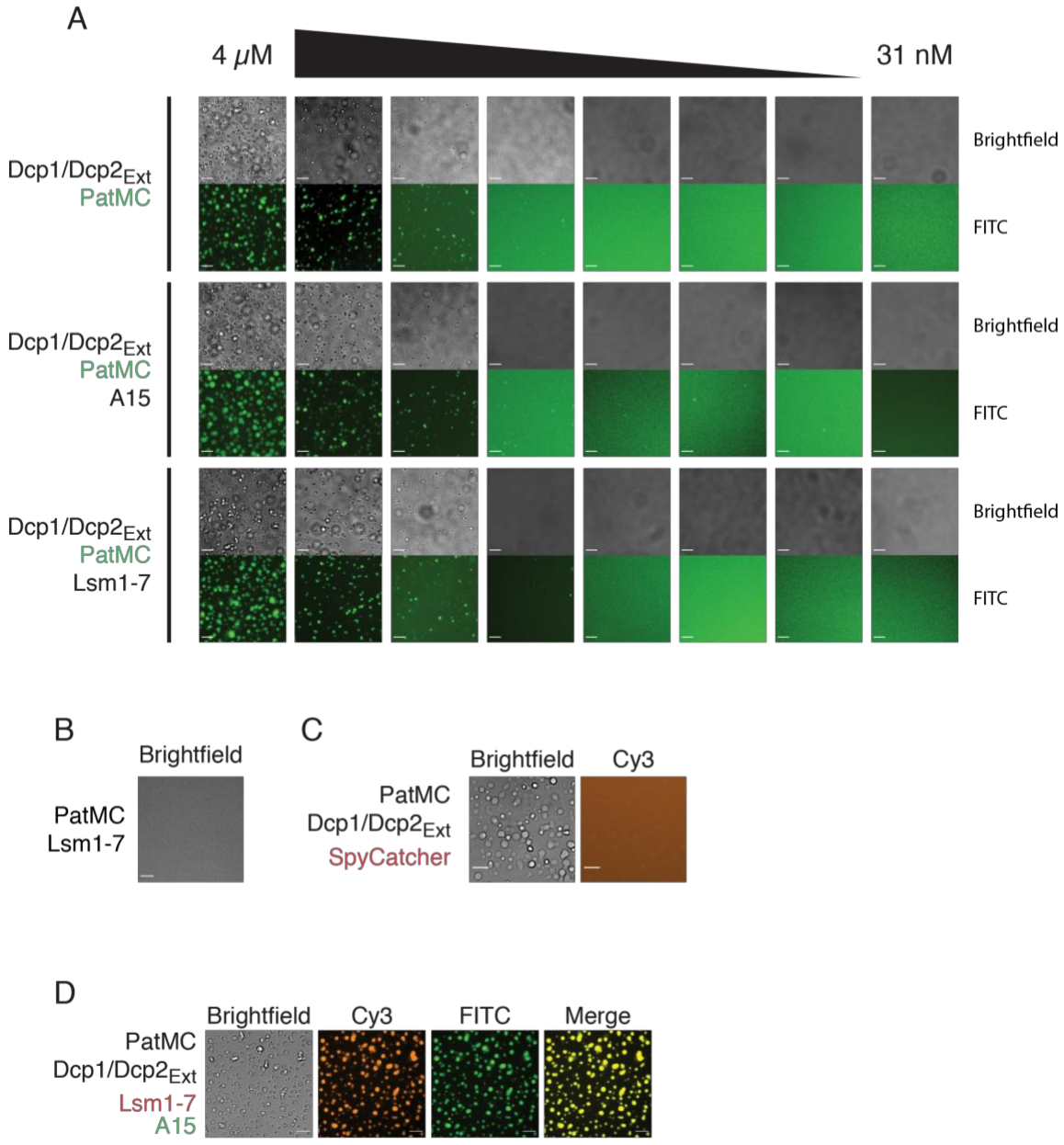

Supplemental Figure 2.5: The multivalent PatMC/Dcp2$_{Ext}$ interaction is required for liquid-liquid phase separation

A, Brightfield images of serial dilutions of droplets containing PatMC/Dcp1/Dcp2$_{Ext}$ with A15 RNA or Lsm1-7. (0.1 μM MBP-PatMC labelled). **B,** Brightfield images of 2.5 μM PatMC and Lsm1-7 **C,** Brightfield and fluorescence microscopy of 2.5 μM MBP-PatMC and Dcp1/Dcp2$_{Ext}$ with 0.1 μM Alexa555-Spycatcher labelled. **D,** Brightfield and fluorescence microscopy of 2.5 μM MBP-PatMC/Dcp1/Dcp2$_{Ext}$/Lsm1-7 droplets with 0.1 μM FAM-rA15 and 0.1 μM Alexa555-Lsm1-7. All images taken at 40x magnification. Scale bar, 10 μm.

Materials and Methods

Protein expression and purification

All proteins were expressed in BL21(DE3)* (Thermofisher) cells in LB media. Cells were grown to OD_{600} = 0.6 at 37 °C, after which IPTG was added to 1 mM. Cells were then grown overnight at 18 °C for 16 hours. For expression of copurified PatMC/Lsm1-7, a polycistron containing all seven Lsm proteins was cloned into site one of a pET-Duet vector, with an N-terminal hexahistidine tag followed by a TEV cleavage sequence on Lsm1. A codon optimized PatMC (residues 296-754) was ordered from IDT and cloned into site two of the pET-Duet vector. Cells were harvested by centrifugation and lysed in appropriate buffer. For Lsm1-7 and PatMC/Lsm1-7 complexes, cells were lysed in Buffer A (2 M NaCl, 20 mM HEPES pH 7.5, 20 mM Imidazole, 5 mM βME, protease inhibitor (Roche)) by sonication. Lysate was subsequently clarified by centrifugation and the supernatant was bound to Ni-NTA resin (GE) at 4 °C for 1 hour. The resin was then transferred to a gravity column and washed with 20 column volumes of Buffer A before being eluted in 25 mL of Buffer E (250 mM NaCl, 250 mM Imidazole, 20 mM HEPES pH 7.0, 10 mM βME). The elution was then loaded directly onto a 5 mL HiTrap Heparin column (GE). The heparin column was run at 2 ml/min from a 0.25-1 M NaCl gradient over 20 column volumes. Fractions containing the appropriate protein complex were concentrated in 30 kD concentrators (Amicon) to ~2 mL before adding TEV overnight at 4 °C. The following day, the sample was filtered and further purified by gel filtration using a Superdex 200 16/60 column (GE). Coexpressed PatMC/Lsm1-7 was purified in 400 mM NaCl, 20 mM HEPES 7.0, 1 mM DTT and Lsm1-7 alone was purified in 150 mM NaCl, 20 mM HEPES pH 7.0, 1 mM DTT. Fractions containing protein were concentrated before being flash frozen and stored at -80 °C.

All MBP-Pat1 fusions were purified as described previously (Lobel et al. 2019). For Spycatcher purification, a C-terminal KCK tag was added (SpycatcherKCK) and purified similar to the MBP-Pat1 fusions, with the heparin step omitted. SpycatcherKCK was purified on Superdex 75 16/60 column in 150 mM NaCl, 20 mM HEPES pH 7.0, 0.5 mM TCEP.

Fluorescence polarization

All fluorescent polarization experiments were performed in 200 mM NaCl, 20 mM HEPES pH 7.0, 1 mM DTT, 5 mM $MgCl_2$ with 0.3 µg/ul Acetylated BSA (Promega) . All RNAs used were labelled with 5' FAM (IDT) and were used at final concentration of 500 pM. All binding curves were fit to the following Hill model for single site binding:

$$Y(mp) = (\max(mp) - \min(mp)) * \frac{[protein]^n}{[protein]^n + {K_d}^n} + \min(mp)$$

To determine the ΔG of binding, each independent replicate was fitted to the above model and ΔG was determined by the relationship ΔG = -RT*ln(k_d). The ΔG from each individual fit was averaged and plotted with standard deviation. Hill coefficients were averaged from fitting three separate binding isotherms and shown with standard deviation.

For stoichiometric analysis, 5'-FAM RNA was kept at 0.5 µM in the same buffer as used for the fluorescence polarization assay. Protein was titrated in and fluorescence polarization was measured for each concentration. The linear portion was fit to a linear model and the average of the last four points were used to fit a line at the saturation point. The intersection of these two lines was used to determine the binding stoichiometry.

Analytical Size Exclusion Chromatography (SEC) and SEC-MALS

Analytical SEC was performed in buffer M (250 mM NaCl, 20 mM HEPES pH 7.0, 1 mM DTT), or in the appropriate NaCl concentration. Samples were mixed at ~30 μM and incubated for 15 minutes in 350 mM NaCl, 20 mM HEPES pH 7.0, 1 mM DTT on ice before being filtered and injected onto a GE Superdex 200 10/300-Increase analytical size exclusion column. When appropriate, samples were mixed with 1.1-fold molar excess RNA. All samples were run at 0.35 ml/min, and peaks were analyzed by SDS-PAGE (Invitrogen). For experiments involving reinjection of fractions over SEC, 500 μl of fractions were spin filtered before reinjecting over SEC.

For SEC-MALS, 165 μg of sample was filtered through a 0.1 μm spin filter (Amicon) before being injected onto a pre-equilibrated KW-804 column (Shodex, New York, New York). For samples with RNA, stoichiometric amounts of RNA were added prior to spin filtration. Data was acquired with an inline DAWN HELEOS MALS and Optilab rEX differential refractive index detector (Wyatt Technology, Santa Barbara, CA). All analysis was performed using ASTRA VI software (Wyatt Technology). Data was then exported and plotted with R.

Analytical ultracentrifugation

Sample was buffer exchanged into buffer M using Zeba spin columns (Thermofisher) and diluted to 9.3 μM. When appropriate, stoichiometric amounts of RNA were added to the sample after buffer exchange. AUC cells were assembled according to manufacturer's protocol and 100 μl of sample was loaded into the cell. The sample was incubated at 22 °C for >2 hours prior to

centrifugation. Samples were run at 30,000 rpm for 10-12 hours in a Beckman XL/A analytical ultracentrifuge. Scans for samples containing only protein were collected at 280 nm, and samples containing RNA were scanned at both 280 and 260 nm. Sedimentation velocity analysis was performed in SEDFIT (NIH) and plots were generated with GUSSI (Schuck 2003; Brautigam 2015). Experimental parameters were determined using SEDNTERP (NIH). The following parameters were used for fitting: partial volume, 0.739818; buffer density, 1.0101; buffer viscosity, 0.0104032.

Protein labelling

For labelling with dyes, proteins were buffer exchanged into appropriate labelling buffer using Zeba spin columns (Thermofisher). Lsm1-7 and SpycatcherKCK were labelled with 5-fold molar excess Alexa Fluor 555 maleimide for one hour at room temperature in 150 mM NaCl, 20 mM HEPES pH 7.5, 0.5 mM TCEP. Reactions were quenched by addition of βME to a final concentration of 10 mM. MBP-PatMC was labelled with 4-fold molar excess NHS-Fluorescein (Thermofisher) for 1 hour at room temperature in 150 mM NaCl, 150 mM Sodium bicarbonate pH 8.4 before being quenched by adding TRIS-HCl pH 8.0 to a final concentration of 50 mM. All quenching steps were performed at room temperature for 20 minutes. Free dye was separated from labelled protein by Illustra NICK columns (GE) according to the manufacturer's instruction. Labelling efficiency and concentrations were calculated by UV-vis spectroscopy.

Microscopy

All images were acquired with Nikon Eclipse T*i* equipped with a 40x dry lens. Samples were prepared in a 384 well plate (Greiner) that was cleaned with 0.1M NaOH and passivated with PEG-

silane and 100 mg/ml BSA (Sigma-Aldrich) before being washing with water to remove residual BSA. Proteins or RNA were mixed at specified concentrations in a final buffer concentration of 60 mM NaCl, 20 mM HEPES pH 7.0, 1 mM DTT. When appropriate, dye-labelled protein or RNA were added to 100 nM. Samples were incubated at room temperature for 20 minutes prior to imaging. Images were analyzed in FIJI (Schindelin et al. 2019).

Acknowledgements

We thank Alexandra Rizo and Serena Sanulli for experimental guidance, the Nikon Imaging Center at UCSF for use of the microscope, and Ryan Tibble and Nathan Gamarra for comments on the manuscript. This work was supported by US National Institutes of Health grant R01GM078360 to J.D.G.

References

Brautigam CA. 2015. Calculations and Publication- Quality Illustrations for Analytical Ultracentrifugation Data. *Methods Enzymol* **562**: 109–133.

Chang H, Lim J, Ha M, Kim VN. 2014. TAIL-seq: Genome-wide Determination of Poly(A) Tail Length and 3' End Modifications. *Mol Cell* **53**: 1044–1052.

Charenton C, Gaudon-Plesse C, Fourati Z, Taverniti V, Back R, Kolesnikova O, Séraphin B, Graille M. 2017. A unique surface on Pat1 C-terminal domain directly interacts with Dcp2 decapping enzyme and Xrn1 5′–3′ mRNA exonuclease in yeast. *Proc Natl Acad Sci* **114**: E9493–E9501.

Chowdhury A, Kalurupalle S, Tharun S. 2013. Pat1 contributes to the RNA binding activity of the Lsm1-7 – Pat1 complex. *RNA* **20**: 1465–1475.

Chowdhury A, Mukhopadhyay J, Tharun S. 2007. The decapping activator Lsm1p-7p-Pat1p complex has the intrinsic ability to distinguish between oligoadenylated and polyadenylated RNAs. *RNA* **13**: 998–1016.

Conti E, Izaurralde E. 2005. Nonsense-mediated mRNA decay: Molecular insights and mechanistic variations across species. *Curr Opin Cell Biol* **17**: 316–325.

Fromm SA, Kamenz J, Noldeke ER, Neu A, Zocher G, Sprangers R. 2014. In vitro reconstitution of a cellular phase-transition process that involves the mRNA decapping machinery. *Angew Chemie - Int Ed* **53**: 7354–7359.

Guo H, Ingolia NT, Weissman JS, Bartel DP. 2010. Mammalian microRNAs predominantly act to decrease target mRNA levels. *Nature* **466**: 835–840.

He F, Celik A, Wu C, Jacobson A. 2018. General decapping activators target different subsets of inefficiently translated mRNAs. *Elife* **7**: 1–30.

Hubstenberger A, Courel M, Bénard M, Souquere S, Ernoult-Lange M, Chouaib R, Yi Z, Morlot

JB, Munier A, Fradet M, et al. 2017. P-Body Purification Reveals the Condensation of Repressed mRNA Regulons. *Mol Cell* **68**: 144–157.e5.

Lim J, Ha M, Chang H, Kwon SC, Simanshu DK, Patel DJ, Kim VN. 2014. Uridylation by TUT4 and TUT7 marks mRNA for degradation. *Cell* **159**: 1365–1376.

Lin Y, Protter DSW, Rosen MK, Parker R. 2015. Formation and Maturation of Phase-Separated Liquid Droplets by RNA-Binding Proteins. *Mol Cell* **60**: 208–219.

Lobel JH, Tibble RW, Gross JD. 2019. Pat1 activates late steps in mRNA decay by multiple mechanisms. *Proc Natl Acad Sci* **116**: 23512–23517.

Mitchell SF, Jain S, She M, Parker R. 2012. Global analysis of yeast mRNPs. *Nat Struct Mol Biol* **20**: 127–133.

Moore MJ. 2005. From birth to death: The complex lives of eukaryotic mRNAs. *Science (80-)* **309**: 1514–1518.

Mugler CF, Hondele M, Heinrich S, Sachdev R, Vallotton P, Koek AY, Chan LY, Weis K. 2016. ATPase activity of the DEAD-box protein Dhh1 controls processing body formation. *Elife* **5**.

Mullen TE, Marzluff WF. 2008. Degradation of histone mRNA requires oligouridylation followed by decapping and simultaneous degradation of the mRNA both 5’ to 3’ and 3’ to 5’. *Genes Dev* **22**: 50–65.

Nissan T, Rajyaguru P, She M, Song H, Parker R. 2010. Decapping Activators in Saccharomyces cerevisiae Act by Multiple Mechanisms. *Mol Cell* **39**: 773–783.

Parker R. 2012. RNA degradation in Saccharomyces cerevisae. *Genetics* **191**: 671–702.

Pei XY, Dendooven T, Sonnleitner E, Chen S, Luisi BF. 2019. Architectural principles for Hfq / Crc- mediated regulation of gene expression. *Elife* **8**: 1–20.

Pilkington GR, Parker R. 2008. Pat1 Contains Distinct Functional Domains That Promote P-Body Assembly and Activation of Decapping. *Mol Cell Biol* **28**: 1298–1312.

Rissland OS, Norbury CJ. 2009. Decapping is preceded by 3' uridylation in a novel pathway of bulk mRNA turnover. *Nat Struct Mol Biol* **16**.

Sachdev R, Hondele M, Linsenmeier M, Vallotton P, Mugler CF, Arosio P, Weis K, Zurich ETH. 2019. Pat1 promotes processing body assembly by enhancing the phase separation of the DEAD-box ATPase Dhh1 and RNA. *Elife* **8**: 1–27.

Schindelin J, Arganda-carreras I, Frise E, Kaynig V, Longair M, Pietzsch T, Preibisch S, Rueden C, Saalfeld S, Schmid B, et al. 2019. Fiji : an open-source platform for biological-image analysis. *Nat Methods* **9**.

Schuck P. 2003. On the analysis of protein self-association by sedimentation velocity analytical ultracentrifugation. *Anal Biochem* **320**: 104–124.

Schutz S, Noldeke ER, Sprangers R. 2017. A synergistic network of interactions promotes the formation of in vitro processing bodies and protects mRNA against decapping. *Nucleic Acids Res* **45**: 6911–6922.

Sharif H, Ozgur S, Sharma K, Basquin C, Urlaub H, Conti E. 2013. Structural analysis of the yeast Dhh1-Pat1 complex reveals how Dhh1 engages Pat1, Edc3 and RNA in mutually exclusive interactions. *Nucleic Acids Res* **41**: 8377–8390.

Sonnleitner E, Wulf A, Pei X, Wolfinger T, Forlani G, Prindl K, Abdou L, Resch A, Allain H, Luisi BF, et al. 2018. Interplay between the catabolite repression control protein Crc , Hfq and RNA in Hfq-dependent translational regulation in Pseudomonas aeruginosa. *Nuc* **46**: 1470–1485.

Stevens a. 1980. Purification and characterization of a Saccharomyces cerevisiae

exoribonuclease which yields 5'-mononucleotides by a 5' leads to 3' mode of hydrolysis. *J Biol Chem* **255**: 3080–5.

Teixeira D, Parker R. 2007. Analysis of P-Body Assembly in Saccharomyces Cerevisiae. *Mol Biol Cell* **18**: 2274–2287.

Tharun S, Parker R. 2001. Targeting an mRNA for decapping: Displacement of translation factors and association of the Lsm1p-7p complex on deadenylated yeast mRNAs. *Mol Cell* **8**: 1075–1083.

Vindry C, Marnef A, Broomhead H, Twyffels L, Ozgur S, Stoecklin G, Llorian M, Smith CW, Mata J, Weil D, et al. 2017. Dual RNA Processing Roles of Pat1b via Cytoplasmic Lsm1-7 and Nuclear Lsm2-8 Complexes. *Cell Rep* **20**: 1187–1200.

Wang C-Y, Wang Y-T, Hsiao W-Y, Wang S-W. 2017. Involvement of fission yeast Pdc2 in RNA degradation and P-body function. *RNA* **23**: 493–503.

Wu D, Muhlrad D, Bowler MW, Jiang S, Liu Z, Parker R, Song H. 2014. Lsm2 and Lsm3 bridge the interaction of the Lsm1-7 complex with Pat1 for decapping activation. *Cell Res* **24**: 233–246.

Wyatt PJ. 1993. Light scattering and the absolute characterization of macromolecules. *Anal Chim Acta* **272**.

Xing W, Muhlrad D, Parker R, Rosen MK. 2018. A quantitative inventory of yeast P body proteins reveals principles of compositional specificity. *bioRxiv*.

Chapter 3

New directions for understanding the function of Pat1

Introduction

The above two chapters outline my major findings for how Pat1 regulates the function and assembly of multiple decay factors. However, I have generated data not included in publication that complements our observations or leads to future directions which may be explored. In the following section, I will outline questions, assays, and pitfalls of several experiments that aim to address the role of Pat1 in activating decapping and promoting droplet formation. Furthermore, I will provide references for additional reagents that may be used to understand how Pat1 functions *in vivo*. Combing these biochemical and genetic approaches will further our understanding of the function of Pat1 in cells.

Results

Distinct regions of Pat1 enhance Lsm1-7 RNA binding and decapping

The experiments in chapter 1 found SLiMs in the middle domain and point mutants in the C-terminal domain that were necessary for Pat1 to enhance Lsm1-7 binding. Pat1 could either have common surfaces and motifs that were required to activate cofactors or contain separate regions that enhance distinct steps during RNA decay. To test this, I queried the ability of PatMCΔLAR or PatMC L457A/E461K to activate decapping. While both these mutants failed to enhance Lsm1-7 RNA binding, they activated decapping to the same extent as wildtype PatMC (**Fig. 3.1**). This suggests that there are distinct regions in both the middle and C-terminal domains required to enhance Lsm1-7 binding and decapping. This could provide evidence for how Pat1 can simultaneously enhance multiple decay factors during decapping.

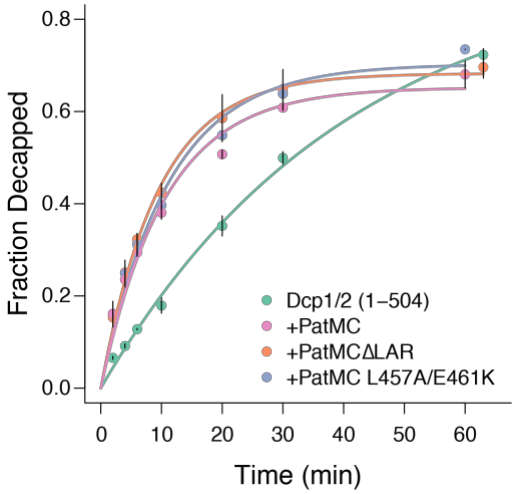

Figure 3.1: PatMC mutants that cannot enhance Lsm1-7 RNA binding still promote decapping
Decapping by Dcp1/Dcp2 (1-504) on a 340mer with an A15 tail. PatMC was kept at 10 µM and Dcp1/Dcp2 was at 0.15 µM.

No synergy between PatMC and Edc3 for activation of decapping by Dcp1/Dcp2

Previous work in the lab has shown that Edc3 also activates Dcp1/Dcp2 in a similar manner to PatMC. To test if there was synergy between Edc3 and PatMC for activating decapping, PatMC alone or in combination with stoichiometric amounts of Edc3 were included in single turnover decapping reactions. PatMC activated decapping to similar extent regardless of the presence of Edc3 (**Fig. 3.2**). This suggests that both Edc3 and PatMC activate through the same mechanism, and inclusion of both does additively promote decapping. This is consistent with genetic data which suggests that PatMC and Edc3 likely regulate a distinct set of transcripts. Edc3, however, is only one of many other known activators of decapping. Future work will test how additional decapping activators may cooperate with PatMC to directly promote decapping.

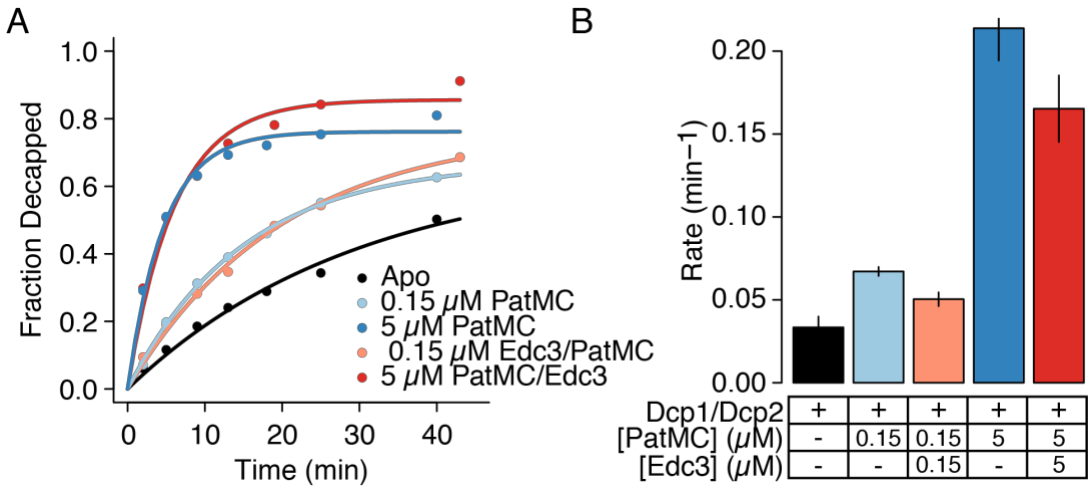

Figure 3.2: PatMC and Edc3 do not synergistically activate Dcp1/Dcp2
A, Decapping reaction with 0.15 µM Dcp1/Dcp2 (1-504) in the presence of either 0.15 or 5 µM MBP-PatMC alone or a MBP-PatMC/Edc3 combination. **B,** Quantification of rates in **A.**

Lsm1-7 inhibits decapping

While the first chapter of this work delineates how Pat1 enhances both 5' and 3' decay factors there was a key experiment which could provide evidence for how Lsm1-7 activates decapping. Clearly Pat1 activates decapping, in part by decreasing K_m, but has relatively weak affinity for RNA on its own. The Lsm1-7 complex is the high affinity RNA binding component, and one would expect it should increase the Dcp1/Dcp2 complex's affinity for RNA. However, addition of Lsm1-7 to the reaction always inhibited decapping in a concentration-dependent manner, regardless of the presence of PatMC (**Fig. 3.3**). Our assays are done under single turnover conditions, where protein concentration greatly exceeds RNA. One possible explanation for the observed inhibition is that the Lsm1-7 complex is 'coating' the RNA and preventing Dcp1/Dcp2 from accessing the substrate. This would prevent catalysis and lead to inhibition. To circumvent these issues, we tried to obtain capping enzyme to create large amounts of RNA substrate, but could never purify the enzyme. Future work requires production of a more capped RNA to perform multiple turnover experiments, which would ensure that Lsm1-7 cannot sequester RNA to outcompete the decapping enzyme.

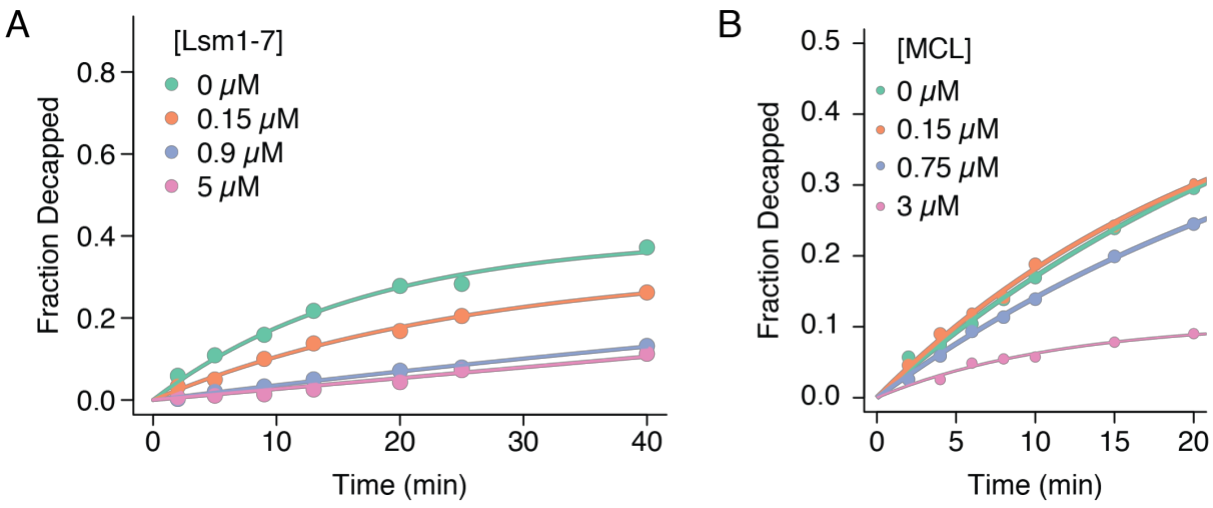

Figure 3.3: Lsm1-7 inhibits decapping by Dcp1/Dcp2
A-B, Increasing concentrations of Lsm1-7 inhibit decapping (**A**), even in the presence of PatMC (**B**). Experiments were performed with Dcp1/Dcp2 (1-504) at 0.15 µM on a 340mer with an A15 tail RNA.

Salt effects on RNA binding and specificity of Lsm1-7 complexes

While chapter 2 outlines how PatMC broadens the specificity of Lsm1-7 for A-rich RNAs, *in vivo* CLIP data suggests Pat1 and Lsm1-7 occupy the 3' ends of mRNAs with no distinguishable sequence motif (Mitchell et al. 2012). Biochemical data from *S.cerevisiae* suggests that the Pat1/Lsm1-7 complex binds A15 RNA with some specificity. However, I tested MBP-PatMC/Lsm1-7 binding to a random fluorescent 12mer RNA (gift from K. Barkovitch) and observed similar binding to the putatively specific A15 oligo (**data not shown**). This suggests that the PatMC/Lsm1-7 does not preferentially bind A15 over heterogenous sequences, consistent with studies reported in chapter 2 (**Fig. 2.1**).

Specific nucleic acid binding involves recognizing the base through π-π interactions and Watson-Crick base-pair mimicry. Nonspecific nucleic acid binding, however, generally involves contacts with the phosphate backbone, or with RNA, the 2' OH on the ribose sugar (Kalodimos et al. 2004).

These ionic interactions are salt sensitive and thus expected to decrease rapidly upon increasing salt concentrations. To test this, MBP-PatMC/Lsm1-7 was kept at 80 nM (~80% K_d) and incubated with either the A15 or 12mer probe. Salt was then titrated into the reaction and the polarization was measured for each salt concentration. Increasing salt concentrations rapidly lead to decrease polarization of the 12mer, indicating dissociation. This effect was less dramatic for A15, which remained bound at higher salt concentrations. This indicates that the PatMC/Lsm1-7 complex can engage diverse heterogeneous sequences; However, base recognition is likely specific for adenine or uracil residues. Understanding how PatMC/Lsm1-7 distinguish specific RNA tails for heterogenous 3' end sequences requires further structural information.

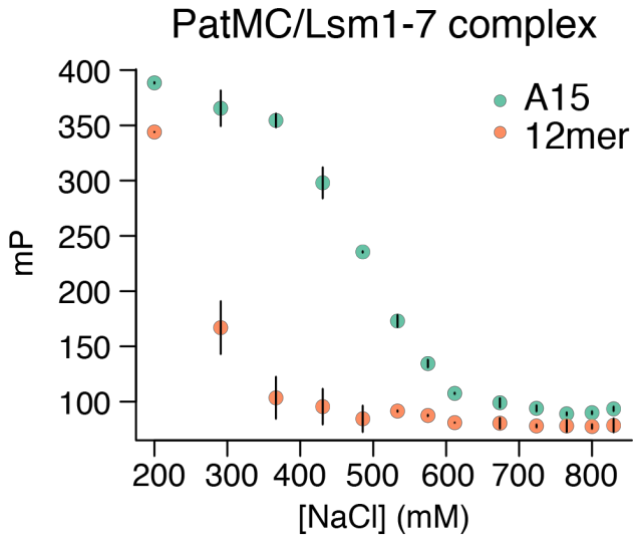

Figure 3.4: A15 RNA binds specifically to the PatMC/Lsm1-7 complex
MBP-PatMC/Lsm1-7 was kept at 80 nM and increasing amounts of NaCl were added to the reaction before measuring fluorescence polarization. 12mer sequence: GCUUUACGGUGC

In the future, one could perform a series of dissociation constant measurements with more fine variations in salt concentration. Then, plotting the log(K_d) vs log([Ionic strength]), one could obtain the number of salt ions used to engaged both specific and non-specific RNA. Performing this in the presence and absence of PatMC could inform if PatMC coordinates additional ions for RNA binding. This may inform on the biophysical mechanism by which PatMC enhances RNA

binding of Lsm1-7. One could also repeat the experiments in chapter 2 **(Fig. 2.1)** to determine how salt affects the specificity of the PatMC/Lsm1-7 complex for adenine vs uracil rich oligoRNAs.

Gaps in knowledge about phase separation

The experiments in chapter 2 of this thesis suggest that RNA promotes a multimeric PatMC/Lsm1-7 complex. Thus, an obvious experiment was to see if addition of Lsm1-7 and RNA to PatMC/Dcp1/Dcp2 droplets decrease the critical concentration required for droplet formation. When a substoichiometric amount of rA15 RNA was added to pre-formed PatMC/Dcp1/Dcp2/Lsm1-7 droplets, the nucleic acid was incorporated into the condensate **(**See chapter 2, **Fig S2.5)**. Stoichiometric amounts of rA15, however, dissolved the droplets (**Fig. 3.5A**). It was exciting to hypothesize that RNA binding somehow prevented droplet formation. As a control, however, addition of dA15 in stoichiometric amounts also dissolved droplets (**Fig. 3.5B**). Dissolution of PatMC/Dcp1/Dcp2/Lsm1-7 droplets by nucleic acids depends on Lsm1-7, as droplets without Lsm1-7 were unperturbed by DNA or RNA (see Chapter 2, **Fig 2.5**). This suggests that nucleic acids work with Lsm1-7 to antagonize droplet formation. One hypothesis is that PatMC uses residues that interact with the phosphate backbone to oligomerize, and when Lsm1-7 and nucleic acid are present, these motifs are obscured and cannot mediate oligomerization. Conformational changes in PatMC associated with nucleic acid binding could also change droplet behavior. In line with this reasoning, we have observed salt dissolves droplets but does not affect HLM binding, suggesting ionic interactions are critical for PatMC/Dcp1/Dcp2 droplets. However, further experiments are required to decipher how Pat1 recognizes nucleic acid with Lsm1-7 in the context of these phase separated droplets.

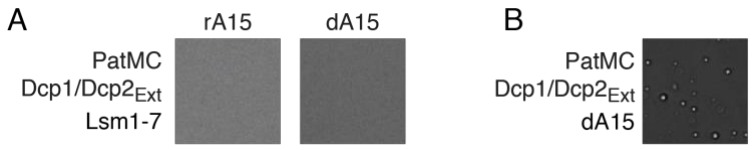

Figure 3.5: Nucleic acids dissolve PatMC/Dcp1/Dcp2 droplets when Lsm1-7 is present
A, Stoichiometric rA15 or dA15 with PatMC/Dcp1/Dcp2/Lsm1-7 droplets. **B,** dA15 does not dissolve PatMC/Dcp1/Dcp2 droplets when Lsm1-7 is absent. All proteins were present at 2.5 μM. Images taken at 40x magnification.

Future work for dissecting the function of Pat1 *in vivo*
The above work outlines a largely biochemical effort to understand the function of Pat1. However, *in vivo* work could complement our biochemical findings or provide new hypotheses to test. The previous *in vivo* work in this thesis examined if Pat1 could function in RNA decay by testing the ability of different truncations to support cell growth. Analysis of mRNA half-lives in these Pat1 strains by northern blots or deep sequencing could provide more information about how different domains affect subsets of Pat1 targets or sequence specificity. Additionally, the role of Pat1 in P-bodies could be examined by using microscopy to determine how different lesions to Pat1 affects P-body formation in *S.pombe*. Furthermore, we do not fully understand the functional consequences of Pat1 oligomerization. Thus, it is of immediate interest to find mutants of Pat1 that can interact with Lsm1-7 or Dcp1/Dcp2 but cannot oligomerize. To do this, one would use a genetic approach to rapidly screen Pat1 constructs defective in P-body formation and then biochemically characterize ones that gave interesting phenotypes.

The above data suggests that the middle domain of Pat1 is necessary and sufficient to promote oligomerization of Pat1. To find regions important for Pat1 oligomerization, I created a series of internal deletions by replacing ~25 residues at a time with a flexible $(GGS)_2$ linker (**Fig. 3.64A, Table 1)**. These PatMC constructs were fused to an MBP tag to enable expression and

electroporated into *S.pombe*. Five of these proteins expressed identically to wildtype PatMC (**Fig. 3.6B)**. An mScarlet-Flag tag was fused to the C-terminus of Dcp1 to be used as a P-body marker. However, a future direction would be to look for lesions in the middle domain that disrupt P-body formation, and then purify interesting constructs and test their ability to enhance Lsm1-7 binding or activate decapping by Dcp1/Dcp2. The combination of genetic and biochemical approaches may provide insight into the functional consequences of oligomerization on both activation and assembly of decay factors.

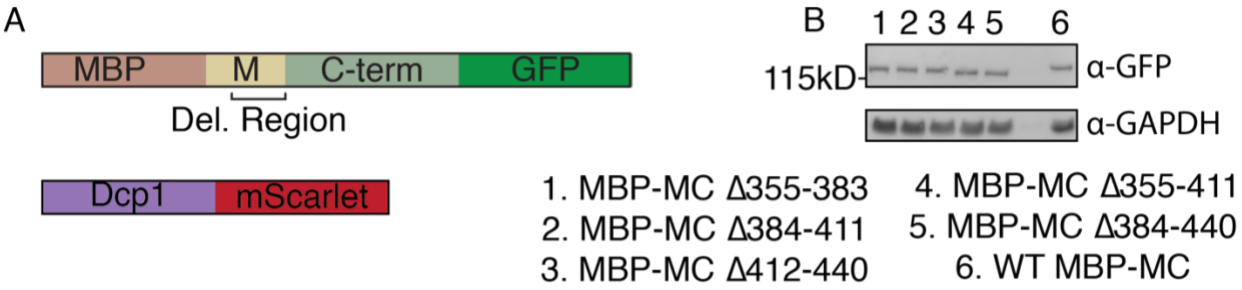

Figure 3.6: Expression of internal PatMC deletions in *S.pombe*
A, Schematic of PatMC and Dcp1 constructs used in study. The Dcp1 construct contains a C-terminal flag tag downstream of the mScarlet fluorescent protein. The region of PatMC that was tiled over for deletions is bracketed and labelled 'Del. Region'. **B,** Western blot of different MBP-PatMC constructs with GAPDH as a loading control. Numbers on top correspond to legend below. Molecular weight marker is shown on left and antibody used to detect is display on right.

Tables

Table 3.1: *S.pombe* strains construct for future use

All contain GFP-tagged Pat1 constructs and mScarlet-flag tagged Dcp1 constructs. Fluorescent tags are appended to the C-terminus of both proteins. Note that strains containing internal deletions are also available in a strain that does not have the Dcp1-mScarlet-flag construct (Data not shown)

Identifier	Strain
spJL029 (FL-Pat)	h+ Δ*Pat1::Pat1:sfGFP:ura4t:HygMX Dcp1::Dcp1:mScarlet:flag:ura4t:NatMX*
spJL030 (MBP-PatMC)	h+ *WT::MBP-Pat296-754:sfGFP:ura4t:HygMX Dcp1::Dcp1:mScarlet:flag:ura4t:NatMX*
spJL031 (PatM)	h+ Δ*Pat1::Pat296-439:sfGFP:ura4t:HygMX Dcp1::Dcp1:mScarlet:flag:ura4t:NatMX*
spJL032 (PatC)	h+ Δ*Pat1::Pat440-754:sfGFP:ura4t:HygMX Dcp1::Dcp1:mScarlet:flag:ura4t:NatMX*
spJL033 (ΔPat1)	h+ Δ*Pat1::KanMX Dcp1::Dcp1:mScarlet:flag:ura4t:NatMX*
spJL034 (MCΔ355-383)	h+ Δ*Pat1::MBP-Pat296-754Δ355-383(GGS)$_2$:sfGFP:ura4t:HygMX Dcp1::Dcp1:mScarlet:flag:ura4t:NatMX*
spJL035 (MCΔ384-411)	h+ Δ*Pat1::MBP-Pat296-754Δ384-411(GGS)$_2$:sfGFP:ura4t:HygMX Dcp1::Dcp1:mScarlet:flag:ura4t:NatMX*
spJL036 (MCΔ412-440)	h+ Δ*Pat1::MBP-Pat296-754Δ412-440(GGS)$_2$:sfGFP:ura4t:HygMX Dcp1::Dcp1:mScarlet:flag:ura4t:NatMX*
spJL037 (MCΔ355-411)	h+ Δ*Pat1::MBP-Pat296-754Δ355-411(GGS)$_2$:sfGFP:ura4t:HygMX Dcp1::Dcp1:mScarlet:flag:ura4t:NatMX*
spJL038 (MCΔ384-440)	h+ Δ*Pat1::MBP-Pat296-754Δ384-440(GGS)$_2$:sfGFP:ura4t:HygMX Dcp1::Dcp1:mScarlet:flag:ura4t:NatMX*

References

Kalodimos CG, Biris N, Bonvin AMJJ, Levandoski MM, Guennuegues M, Boelens R, Kaptein R. 2004. Structure and Flexibility Adaptation in Nonspecific and Specific Protein-DNA Complexes. *Science (80-)* **305**: 386–389.

Mitchell SF, Jain S, She M, Parker R. 2012. Global analysis of yeast mRNPs. *Nat Struct Mol Biol* **20**: 127–133.

Conclusion

This work provides a mechanistic framework for understanding how Pat1 regulates the activity, specificity, and assembly of multiple mRNA decay factors. First, I showed how Pat1 uses a bipartite interaction of its middle and C-terminal domains to promote distinct steps of decapping by recruiting Lsm1-7 to RNA and enhancing cap hydrolysis by Dcp1/Dcp2. Second, Pat1 broadens the substrate selectivity of the Lsm1-7 by increasing its affinity for A-rich RNAs. Third, Pat1 oligomerizes to promote higher order assembly of Pat1/Lsm1-7 complexes, which is potentiated by RNA binding. Last, the inherent oligomerization of Pat1 triggers phase separation with multivalent cofactors, such as the Dcp2 enzyme containing multiple HLMs. Taken together, this work uncovers the critical molecular features of Pat1 that enable it to regulate multiple mRNA decay factors and coordinate the assembly of a decapping mRNP.

We sought to understand how the middle domain of Pat1 promotes 5'-3' RNA decay. Our *in vitro* reconstitution approach revealed that, in conjunction with PatC, PatM uses two SLiMs to activate RNA binding by Lsm1-7 by promoting a protein-protein interaction and stabilizing a high affinity RNA binding conformation by an unknown mechanism. This clarifies one mechanism for how the essential middle domain controls decapping. The enhancement of Lsm1-7 is sequence specific; on its own, Lsm1-7 strongly prefers binding U-rich substrate, but addition of Pat1 dampens this effect by enhancing binding to A-rich substrates. Thus, Pat1 may serve as a specificity factor for recruiting Lsm1-7 to suboptimal target RNAs. Future work aims to understand the molecular details about how Pat1 broadens sequence recognition of the Lsm1-7 complex.

Pat1 also uses a combination of the middle and C-terminal domain to active decapping by Dcp1/Dcp2. The C-terminal domain binds HLMs in Dcp2, but is unable to activate decapping on

its own. However, PatC contains two functional regions required to activate decapping. First, it binds HLMs with a unique fungal extension and contains a basic patch that cooperates with the middle domain to promote decapping. Thus, PatC plays a role in both binding Dcp2 and, in conjunction with the middle domain, activating decapping. Pat1 can also activate decapping by two mechanisms, by either 1) increasing the affinity of Dcp1/Dcp2 for substrate or 2) alleviating autoinhibition to promote catalysis. Furthermore, the regions required to activate decapping are separable from those required to enhance Lsm1-7 RNA binding, suggesting that Pat1 uses multiple regions and surfaces to activate distinct steps of mRNA decay. This multifunctionality may inform on how Pat1 can regulate multiple post-transcriptional events, which requires further mechanistic analysis in cells.

In addition to activating decay factors, our biochemical work has uncovered how Pat1 can regulate the assembly of its interaction partners. First, the discovery that RNA induces multimerization of the PatMC/Lsm1-7 complex revises our understanding of how the heterooctamer may be engaging the complex. It has been previously thought that one heterooctamer engages RNA. Our biochemical results suggest that multiple Pat1/Lsm1-7 complexes can simultaneously bind RNA. Mechanistically, we cannot yet distinguish if multiple Pat1/Lsm1-7 complexes co-occupy a single long RNA, or if the dimer of heterooctamers can bind multiple different RNAs. Immediate work will aim to understand the thermodynamic framework and RNA targets of oligomeric Pat1 complexes to resolve the order of assembly. Additionally, the assembly of Pat1 is tuned by its interaction partners. While Lsm1-7 promotes formation of Pat1 assemblies with defined size and stoichiometry, Dcp2 promotes condensate formation of heterogenous sizes. These droplets can recruit both 5’ and 3’ RNA decay factors, which may be leveraged for 5’-3’ end communication

during mRNA turnover. However, more work is required to determine the activity of factors inside the droplets and how this is modulated by the protein compostion. Understanding how different decay factors and substrates regulate oligomerization of Pat1 requires characterization of assemblies with additional interaction partners.

This work dissects how Pat1 functions with two important decay factors. However, Pat1 clearly has roles beyond these steps. Future work will aim to define how Pat1 interacts with and modulates the activity of other interaction partners such as the DEAD-box helicase Dhh1 or the CCR4/NOT deadenylation complex. In addition to understanding how Pat1 regulates individual decay factors, our discovery of an oligomeric Pat1 complexes suggests that cofactors tune the assembly of Pat1. Cataloging how different decay factors change the assembly of Pat1 both *in vivo* and *in vitro* will further elucidate the role of oligomerization for the function of Pat1. Towards this end, we are at a point where many different mRNA decay factors from *S.pombe* have been biochemically characterized. It is of great interest to now test how combinations of factors modulate each other's activities and assemblies. Future research will use a combination of biochemical, structural, genetic, and cell biological approaches to understand how Pat1 functions in a dense network of protein-protein interactions to regulate decapping. Ultimately, this will lead to a complete mechanistic understanding about how 5' and 3' decay factors communicate during bulk RNA turnover.

Publishing Agreement

It is the policy of the University to encourage open access and broad distribution of all theses, dissertations, and manuscripts. The Graduate Division will facilitate the distribution of UCSF theses, dissertations, and manuscripts to the UCSF Library for open access and distribution. UCSF will make such theses, dissertations, and manuscripts accessible to the public and will take reasonable steps to preserve these works in perpetuity.

I hereby grant the non-exclusive, perpetual right to The Regents of the University of California to reproduce, publicly display, distribute, preserve, and publish copies of my thesis, dissertation, or manuscript in any form or media, now existing or later derived, including access online for teaching, research, and public service purposes.

DocuSigned by:
09B696F68EAB415...
Author Signature

3/12/2020
Date